https://doi.org/10.5194/egusphere-2026-3399
Preprint. Discussion started: 19 June 2026

Earthquake Scaling Equations Under Small Strain, Steady Moment Release-Rate Conditions in Southern Andes from 2015 to 2017

Patricio A. Toledo[1], Cristián Siegel[2], Benoit Derode[3], Raúl Madariaga[1,4], and Jaime Campos[1,5]

[1]Programa Riesgo Sísmico PRS, Universidad de Chile, Blanco Encalada 2002, Santiago, Chile.
[2]GFZ Helmholtz Centre for Geosciences, Potsdam, Germany
[3]Institut Terre et Environnement Strasbourg, EOST, Université de Strasbourg/CNRS, Strasbourg, France
[4]Département de Géologie, Ecole Normale Superieure, PSL University, 75005 Paris, France.
[5]Departamento de Geofísica, Facultad de Ciencias Físicas y Matemáticas, Universidad de Chile, Beauchef 850, Santiago, Chile.

Correspondence: Cristián Siegel (cristian.eduardo.siegel.giraud@gfz.de)

Abstract. In the South Andes western edge, a very active seismic contact, with earthquakes up to magnitude 9.5 and ca. $4000\ \mathrm{km}$ in length threatens cities and very large populations. The existence of modern seismological networks along the contact allowed the observation of unprecedented earthquake cycle characteristics, which can improve our ability to estimate earthquake hazard, a main objective of seismology. Using dimensional and similarity analysis techniques, we show precise mechanical conditions under which the earthquake generation process unfolds, and theoretically-derive a set of scaling equations linking renormalized variables. Later on, we test our theoretical results using a curated earthquake point-catalog by using gridding, box-counting, statistical bootstrap and fixed-point iteration collapse techniques. We found non-trivial scaling laws valid across multiple orders of magnitude capable of describing a complex interplay between renormalized earthquake occurrence and renormalized seismic-moment release-rate. We discuss implications in terms of small-strain and seismic-moment release-rate imposed; cutoff magnitudes, statistical properties of seismicity, how seismic cycle might be analyzed in presence of long-term correlations, seismic-moment transfer under small-strain conditions, earthquake hazard implications and tectonic status. Finally, we conclude that exponents characterizing seismicity are related through a set of scaling equations, meaning that all considered processes have very long-term correlations. The available data suggests a single power law fitting data across the western edge. These equations were obtained by an asymptotic analysis, also a cascade mechanism is proposed to explain the observed moment release behavior.

1 Introduction

At the western edge of South America two plates subduct, the Nazca Plate to the north and the Antarctic Plate to the south (Ranero et al., 2006). This configuration defines the Southern Andes as one of the seismic zones with the greatest length and seismic activity, far exceeding $4000\ \mathrm{km}$ long, where earthquakes up to magnitude 9.5 (Ruiz and Madariaga, 2018) have been recorded. In Chile, this condition directly affects large communities. For instance Camus et al. (2016) estimated an affected population of 11 million in 2010 only. Therefore, knowing the behavior of seismicity presents a fundamental scientific

https://doi.org/10.5194/egusphere-2026-3399
Preprint. Discussion started: 19 June 2026

challenge, and at the same time a practical public policy issue. The precise determination of statistical laws and conditions under which the earthquake generation process unfolds requires theory and experimental observations, and advances in one area or another has positive implications in earthquake hazard analysis. Taking advantage of the unique opportunity that this geographic area represents, during the last decades large instrumental network-installation and maintenance efforts have been put in-place that have made the construction of earthquake point-catalogs possible, allowing exploration of previously unobserved properties over a greater dynamic range of source dimensions. Therefore, it is expected that these new observations will lead to new extended laws that will improve our understanding of the processes occurring in the crust, and ultimately improve our ability to estimate earthquake hazard.

In connection to hazard is the notion of seismic cycle and the proper-length scale attached to it, naturally the largest scale is intensely studied because it determines the maximum credible earthquake, relevant in hazard studies. For example, on the western edge of the Andes, between 18 and $24°\mathrm{S}$ latitude Métois et al. (2013) have established a series of segments, whose proper-lengths are believed to have some predictive power when analyzing the geodetic coupling. Similarly between 26 and $30°\mathrm{S}$ latitude, there is a well known segment, quiescent since the 1922 $Mw\,8.6$ earthquake (Ruiz and Madariaga, 2018). These segments, approximately $500\ \mathrm{km}$, are associated with return periods ca. $100\ \mathrm{years}$, therefore it is natural to inquire about the relationship among those quantities.

We then face a problem of maximum earthquake size, occurrence time and affected area. We should add a degrees-of-freedom dimension, as geological evidences have shown that interaction between crust faults plays a fundamental role (King et al., 1994; King and Cocco, 2001). A simple tool much used when no firm theoretical foundations are available is dimensional analysis. It is based on well known mathematics as group theory and geometrical similarity, nonetheless its consequences are deep. It allows determination of general relationships between relevant physical parameters and most of the times a simplification in terms of number of variables involved (Bridgman, 2007; Zorich, 2010; Barenblatt, 1996).

Central to the idea of analyzing the particular behavior of the phenomenon by means of dimensionless variables, is the existence of an *intermediate asymptotics*, that is, the regime where the phenomenon is sufficiently far from the initial conditions but at the same time it is far enough from its final equilibrium state. To cite an example, Kostrov's solution to the circular fault growth problem is bounded by two well-defined boundaries, on the one hand are the phenomena that take place in the process zone at the tip of the fault, which correspond to rather microscopic lengths, and on the other hand are the phenomena that take place at the edges of the fault which are macroscopic lengths. Between both boundaries, there is a *length range* where the fault grows in a self-similar way, whose scale laws dominate and which corresponds to the intermediate asymptotics of the phenomenon. Thus, it follows that by analyzing the asymptotic behavior of the variables, which are local conditions of the problem at hand, it is possible to establish or discard the appearance of this privileged regime. For a detailed description of the intermediate asymptotics idea as well as multiple applications see Barenblatt (2014).

Our paper is organized as follows: In Section 2 we describe the problem of seismicity generation framed in a seismic-moment loading-unloading cycle. We then extract precise conditions, based on observations, to simplify the problem and make the main similarity assumptions. Then we propose scaling relationships. This set of novel equations represent the correlations developed as the seismicity phenomenon unfolds. Section 3 presents a review of the tectonic context in which the scaling

https://doi.org/10.5194/egusphere-2026-3399
Preprint. Discussion started: 19 June 2026

equations are intended to be applied, and describes the existing instrumentation and data set. Subsequently, the methodological and statistical elements used to process the earthquake point-catalog information are shown in Section 4. In Section 5 the results are presented and the scaling characteristics and properties are given. In Section 6 various implications regarding hypothesis made, treatment of earthquake data, catalog properties, earthquake interaction (seismic-moment transfer), seismotectonics processes, and earthquake hazard are raised. In Section 7 several relevant conclusions are drawn.

2 Problem setting

As the Earth's crust is the place where the earthquake generation process takes place, let us consider a region $\mathcal{R}$ (Figure 1) where the main elements in consideration are set. Let us parameterize the crust by considering the class of systems of units where seismic-moment, length and time (MLT) are used to describe the quantities of interest. Thus, for example, forces are measured in units of seismic-moment per unit length, energy and work are measured in units of seismic-moment and power is measured in units of seismic-moment per unit time. We suppose that the crust is characterized by a seismogenic thickness H. A certain power R —the main source of available energy— is injected into the crust from the heat flux through Earth's mantle and it is applied at ocean expansion rifts over a very long time T as a tectonic loading process. A fraction Q of the injected power R is freed when, as time goes by, crust-faults slip a certain amount u releasing a stress-drop $\Delta\sigma$, producing earthquakes whose sizes are measured through a scalar seismic-moment Mo. Therefore Q represents a seismic-moment release-rate, this way, there is a residual energy budget that might account for a wide spectrum of motions known (Ide et al., 2007) not measured in earthquake point-catalogs. In general $Q \leq R$, and for many cycles of a characteristic earthquake size, an interevent time distribution might be estimated by $\tau = Mo/R$, and this recurrence phenomenon can be consecutive events located in the same place (first-return events) or scattered at a distance ℓ (all-return events) within the region bounds. It follows that n, τ, ℓ and Mo are random variables over $\mathcal{R}$, and given that the region of interest might change, these variables better be considered in full generality as random-field processes.

As a hazard approximation, we wish to estimate the number of events per unit time and unit area n taking place in the given geographic region of interest $\mathcal{R}$, during the observation period T given by a general relation φ linking n and the aforesaid parameters:

$$n = \varphi\left(\ell, \tau, \Delta\sigma, T, Mo, H, u, Q\right). \tag{1}$$

Table 1 shows powers of the dimension function for each parameter, for instance, the dimensions of the number of events distribution are $[n] = \mathrm{L}^{-2}\ \mathrm{T}^{-1}$, the dimensions of the stress-drop are $[\Delta\sigma] = \mathrm{M}\ \mathrm{L}^{-3}$, the dimension of the interevent distance is $[\ell] = \mathrm{L}$, and the dimension of the interevent time is $[\tau] = \mathrm{T}$.

Thus, the number of events distribution n is a function of 8 parameters. As MLT has 3 independent units, there are 3 quantities with dimensions that might be considered independent, let us choose $\Delta\sigma, \ell$ and τ. Therefore, there are $m = 5$ parameters with dependent dimensions. According to dimensional analysis (Sedov, 1993) a function Φ exists such that:

$$\frac{n}{\ell^{-2}\tau^{-1}} = \Phi\left(\frac{T}{\tau}, \frac{Mo}{\Delta\sigma\ell^3}, \frac{H}{\ell}, \frac{u}{\ell}, \frac{Q}{\Delta\sigma\ell^3\tau^{-1}}\right), \tag{2}$$

https://doi.org/10.5194/egusphere-2026-3399
Preprint. Discussion started: 19 June 2026

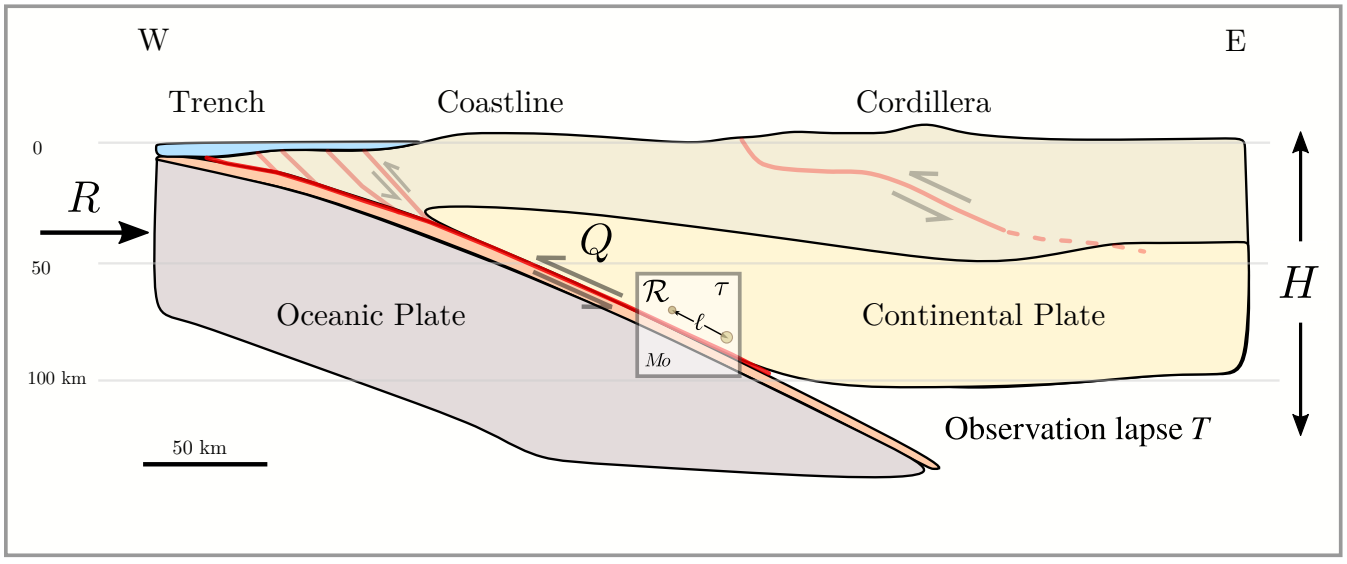

Figure 1. Cross section sketch of a subduction border. An energy injection is placed west with a power R, feeding a complex tectonic process with characteristic geomorphologies (trench, coastline and cordillera) induced by a Continental Plate overriding an Oceanic Plate. Within a region $\mathcal{R}$, random variables ℓ, τ and Mo characterize an earthquake process with rate Q across a larger volume with proper-length H. The observation period T determines the longer time periods available for study. Depths and graphic scale as indicated.

Table 1. Powers of the dimension function in the MLT class for each parameter used in text. Note that n has flux units and $\Delta\sigma$ has density of moment units.

	n	ℓ	τ	$\Delta\sigma$	T	Mo	H	u	Q
M	0	0	0	1	0	1	0	0	1
L	−2	1	0	−3	0	0	1	1	0
T	−1	0	1	0	1	0	0	0	−1

which is a general result obtained from units alone. In mathematical terms, Φ is symmetric with respect to a group of transformations defining change from one system of units to another within a given class of systems of units. In physical terms, meaningful laws cannot depend on the choice of units, therefore it must be possible to express them using relationships between quantities that do not depend on this arbitrary choice, i.e. dimensionless combinations of variables.

Let us introduce the dimensionless quantities:

$$\Pi = \frac{n}{\ell^{-2}\tau^{-1}}, \quad \Pi_T = \frac{T}{\tau}, \quad \Pi_{Mo} = \frac{Mo}{\Delta\sigma\ell^3},$$
$$\Pi_H = \frac{H}{\ell}, \quad \Pi_u = \frac{u}{\ell}, \quad \Pi_Q = \frac{Q}{\Delta\sigma\ell^3\tau^{-1}},$$

https://doi.org/10.5194/egusphere-2026-3399
Preprint. Discussion started: 19 June 2026

The relation (2) might then be expressed as follows:

$$\Pi = \Phi\left(\Pi_T, \Pi_{Mo}, \Pi_H, \Pi_u, \Pi_Q\right), \tag{3}$$

If we would like to obtain the earthquake occurrence probability distribution, that is to say to sample the distribution Π, we should explore a space of 5 dimensions, one for each dimensionless quantity. If we consider 10 independent observations to estimate the expected value of these dimensionless quantities, we get that an earthquake point-catalog should have at least 10^5 observations, reasonable smaller than 10^8 elements of the original formulation in Eq. (1).

2.1 Complete similarity conditions

On a physical level a parameter is considered essential, i.e. governing the phenomenon, if the value of the corresponding dimensionless parameter is not too large or not too small (about 0.1 and 10). Thus, let $l \leq m$ define a subset of the parameters. If the dimensionless parameters $\Pi_{l+1}, \ldots, \Pi_m$ are small or large, it is assumed by convention that the influence of these dimensionless parameters, and consequently of the corresponding dimensional parameters, can be neglected (for a discussion and theorems sustaining this procedure see Barenblatt (2003)). If these conditions are actually satisfied for sufficiently small or sufficiently large $\Pi_{l+1}, \ldots, \Pi_m$ the function $\Phi(\Pi_1, \ldots, \Pi_l, \Pi_{l+1}, \ldots, \Pi_m)$ can be replaced by a function Φ^* with fewer arguments:

$$\Pi = \Phi^*\left(\Pi_1, \ldots, \Pi_l\right). \tag{4}$$

In such cases, we speak of *complete similarity* or *similarity of the first kind* of a phenomenon in the parameters $\Pi_{l+1}, \ldots, \Pi_m$ (Barenblatt, 1987).

Below, we review for each of the dimensionless parameters in Eq. (3) their asymptotic behavior. Such that when these parameters are reasonably bounded around 1 they are considered governing parameters, i.e. kept in the physical model and when these parameters goes to zero or infinity, a similarity hypothesis will be made.

The observational period T and the interevent times τ define Π_T, it happens that Π_T is the inverse of Deborah number De^{-1}, used in very-short or very-long term rheology experiments (Huilgol and Phan-Thien, 1997; Mendecki, 1996). Deborah number is the ratio between the characteristic relaxation (response) time of a body subjected to a load, and the process loading-time duration itself, thus for $De \ll 1$ the body behaves like a liquid and for $De \gg 1$ like a solid. The parameter Π_T represents a normalized frequency and poses a very common problem in seismology and geodesy, that is the fact that the tectonic seismic-moment release process spans millions of years, meanwhile modern earthquake point-catalogs are only decades long (Mueller, 2019). Although historical data might increase the observation period to hundreds of years (Lomnitz, 1970, 2004; Udías et al., 2012) and paleoseismology to thousands (Cisternas et al., 2012; Vargas et al., 2014) in most scenarios Π_T is very uncertain. In practice, for an open observation period we cannot know which events have interevent times much smaller than the observation period. Thus a noticeable number of earthquake pairs will have interevent times τ as large as the observation period T, therefore $\Pi_T \simeq 1$. This parameter cannot be neglected.

The dimensionless parameter Π_{Mo} is discussed by Golitsyn (2007, 2001). The factor $Mo/\Delta\sigma$ represents, according to Tsuboi (1940) and Tsuboi (1956), a representative volume where seismicity takes place. Thus, every earthquake is endowed with a

https://doi.org/10.5194/egusphere-2026-3399
Preprint. Discussion started: 19 June 2026

proper-length scale $\sqrt[3]{Mo/\Delta\sigma}$ (Aki, 1972; Kostrov, 1974). It has been known for a while the remarkable low fluctuations of $\Delta\sigma$, and various scaling laws can be derived from this observation (Kanamori and Anderson, 1975; Aki, 1967). A common value for stress-drop is $\Delta\sigma \simeq 4$ MPa (Allmann and Shearer, 2009; Yoshimitsu et al., 2014; Goodfellow and Young, 2014), thus if stress-drop is nearly constant, then the seismic-moment should scale with the cube of this length scale (Madariaga, 1979) and Π_{Mo} is expected to fluctuate heavily in earthquake point-catalog surveys, displaying very large and very small values never approaching an asymptotic limit and then cannot be neglected.

The parameter Π_H plays a role similar to inverse Knudsen Kn^{-1} number in statistical physics (Rapp, 2016). It is the ratio of seismogenic thickness H controlling the spatial region of interest and the interevent distance ℓ. Π_H represents a normalized wavenumber. For most earthquake pairs ℓ will be small compared to H, so Π_H should be very large, but long-range space correlations (Kagan and Knopoff, 1980) implies that a considerable number of earthquake pairs will have interevent distances comparable with the seismogenic thickness, therefore $\Pi_H \simeq 1$ remains essential (Aki, 1996) and cannot be neglected.

The dimensionless parameter Π_Q represents the seismic-moment release-rate process. This governing parameter is the most uncertain variable, as our current earthquake point-catalogs only contains very gross information, in practice we estimated Q by the total seismic moment released divided by the observation period, so that $Q \simeq 1.50 \cdot 10^{12}$ W. The fault slip u is a parameter that scales with the seismic-moment with a power-law (Aki, 1972) thus Π_u is not expected to be constant, but as long as the interevent distance ℓ remains long enough compared with fault slip, this parameter, that represents a finite strain, will be small. In simple words, given an earthquake pair with interevent distance ℓ, if one of them is very large in size, such that its fault-length is much greater that ℓ, then its pair might be considered stationary and likely not influence whatever in-place interaction mechanism present. It is therefore natural to introduce a *first similarity hypothesis* regarding small finite strains and propose a further simplification of Eq. (3):

$$\Pi = \Phi^* \left(\Pi_T, \Pi_{Mo}, \Pi_H, \Pi_Q\right), \tag{5}$$

i.e. based on observational facts, we claim there is complete similarity in the parameter Π_u. We expect therefore the function Φ to converge —fast enough— to a non-zero limit Φ^* when the aforementioned dimensionless quantity goes to zero.

2.2 Incomplete similarity conditions

The situation just described is far from being the general case. According to Barenblatt (2003) when the dimensionless parameters $\Pi_{l+1}, \ldots, \Pi_m$ go to zero or infinity the function Φ does not necessarily tend to a limit. Therefore, the physical parameters remain essential, no matter how small or large the values of the corresponding dimensionless parameters $\Pi_{l+1}, \ldots, \Pi_m$ are. It just happens that there exists another class of phenomena, wider that the class of *complete similarity* phenomena, where the function Φ have at large or small values of $\Pi_{l+1}, \ldots, \Pi_m$ the property of generalized homogeneity in its own dimensionless arguments:

$$\Phi = \Pi_{l+1}^{\alpha_{l+1}} \cdots \Pi_m^{\alpha_m} \Phi^* \left(\frac{\Pi_1}{\Pi_{l+1}^{\beta_1} \cdots \Pi_m^{\delta_1}}, \ldots, \frac{\Pi_l}{\Pi_{l+1}^{\beta_l} \cdots \Pi_m^{\delta_l}} \right), \tag{6}$$

https://doi.org/10.5194/egusphere-2026-3399
Preprint. Discussion started: 19 June 2026

where $\alpha_{l+1},\ldots,\alpha_m,\beta_1,\ldots,\delta_l$ are unknown exponents. Equation (3) comes from (group) covariance of meaningful physical laws under a change of units, on the other hand the generalized homogeneity of Eq. (6) is a particular property. The exponents cannot be obtained, even in principle, by dimensional considerations, i.e. they are not universal and they depend on specific conditions of the problem under study. The parameters $\Pi_{l+1},\ldots,\Pi_m$ —which are violating complete similarity— do not disappear from the analysis, they continue to remain essential, no matter how large or small its similarity parameters are. We say the solutions *scale* with the dimensionless quantities $\Pi_{l+1},\ldots,\Pi_m$. As proposed by Zel'dovich (1956), in such cases we speak of *incomplete similarity* or *similarity of the second kind* in the relevant parameter. Often, the exponents are obtained by fitting experimental results, observations, or by numerical modeling. They tend to be real non-rational values, physicists call these exponents *anomalous dimensions* (Wilson, 1975) and the scaling procedure bears the name *renormalization* (Kadanoff, 1966) which is a by-product of covariance of Φ^* under rescaling of its own dimensionless arguments (Goldenfeld, 1992).

Starting from early models of seismicity viewed as critical systems (Main, 1996) and beginning with the work of Bak et al. (2002); Christensen et al. (2002) and the research of Kossobokov and Mazhkenov (1994) a systematic generalization of earthquake scaling relations took place. It is now recognized that a wider set of laws rule the seismic-moment release-rate process in the crust (Corral, 2003). Equation (5) expresses earthquake occurrence statistics under very restricted complete similarity conditions. Extensive observational data describing long-period interevent time correlations (Omori, 1894; Utsu et al., 1995; Ogata, 1988; Jones and Molnar, 1979) suggests that there is incomplete similarity in the parameter Π_T under conditions of large (and small) values of the dimensionless parameter, that is:

$$\Pi = \Pi_T^{\alpha}\Phi^*\left(\frac{\Pi_{Mo}}{\Pi_T^{\alpha_{Mo}}},\frac{\Pi_H}{\Pi_T^{\alpha_H}},\frac{\Pi_Q}{\Pi_T^{\alpha_Q}}\right), \tag{7}$$

where $\alpha,\alpha_{Mo},\alpha_H$ and α_Q are real-valued exponents. Analogous conditions over seismic-moment dimensionless parameter Π_{Mo} are well known (Gutenberg and Richter, 1956):

$$\Pi = \Pi_T^{\alpha}\Pi_{Mo}^{\beta}\Phi^*\left(\frac{\Pi_H}{\Pi_T^{\alpha_H}\Pi_{Mo}^{\beta_H}},\frac{\Pi_Q}{\Pi_T^{\alpha_Q}\Pi_{Mo}^{\beta_Q}}\right), \tag{8}$$

where β,β_H, and β_Q are real-valued exponents also. Similar evidence regarding long-range interevent distance correlations (Kagan and Knopoff, 1980; Scholz and Aviles, 1986; Okubo and Aki, 1987), as well as (renormalization) group symmetries (Corral, 2005) suggests that under conditions of large (or small) values of the similarity parameter Π_H, incomplete similarity exists, that is:

$$\Pi = \Pi_T^{\alpha}\Pi_{Mo}^{\beta}\Pi_H^{\gamma}\Phi^*\left(\frac{\Pi_Q}{\Pi_T^{\alpha_Q}\Pi_{Mo}^{\beta_Q}\Pi_H^{\gamma_Q}}\right), \tag{9}$$

with γ and γ_Q real-valued exponents. Rearranging terms, a symmetrical form might be obtained that can be interpreted in terms of renormalized parameters only:

$$\Pi^* = \Phi^*(\Pi_Q^*), \tag{10}$$

where Π^* is the renormalized event number and Π_Q^* is the renormalized seismic-moment release-rate number. Thus, the Eq. (10) represents a *second similarity hypothesis*, regarding long-range correlation conditions. We must remark that exponents

https://doi.org/10.5194/egusphere-2026-3399
Preprint. Discussion started: 19 June 2026

$\alpha, \beta, \gamma, \alpha_Q, \beta_Q$, and γ_Q define events number distribution given the particular seismic conditions (interevent times, interevent distances, seismic-moment, seismic-moment release-rate), tectonic conditions (stress-drop and seismogenic width) and other region-dependant parameters (observation period). Note that constancy of Q lead us to a *third hypothesis* regarding steady seismic-moment release-rate conditions.

2.3 Scaling equations

Going back to the original variables in Eq. (9) we might write a formulation in dimensional form:

$$n\tau^p Mo^b \ell^d = f(\tau^{p_Q} Mo^{b_Q} \ell^{d_Q}), \tag{11}$$

where f is a scaling function depending on tectonic conditions at play. We remark that all three hypothesis regarding similarity and seismic-moment release rate are already taken into account. We can compare term by term Eq. (9) and (11) and obtain:

$$\begin{cases} p = \alpha + 1, & b = -\beta, & d = 3\beta + \gamma + 2, \\ p_Q = \alpha_Q + 1, & b_Q = -\beta_Q, & d_Q = 3\beta_Q + \gamma_Q - 3. \end{cases} \tag{12}$$

Which translates the specific properties of the problem from dimensionless variables to exponents. These conditions are termed scaling relations, and represent fundamental objects in critical phenomena theory (Widom, 2009). In our interpretation, these scale equations represent the intermediate asymptotics regime where seismicity is ruled by power laws. The exponent p controls time correlations between events, it is indirectly related to Omori law (Godano, 2015), d is related to epicenters fractal dimension (Scholz and Aviles, 1986) and b is related to seismic moment scaling (Kanamori and Anderson, 1975). Note that Gutenberg-Richter balance exponent b_{GR} is defined with respect to survival (complementary cumulative) magnitudes, and as we use seismic-moments we have $b = \frac{2}{3} b_{\mathrm{GR}}$ (Serra and Corral, 2017). Also note that using cumulative experimental histograms avoids $1 + \beta$ exponents that are source of confusions (Kagan, 1994). When Φ^* is linear, exponents p_Q, d_Q and b_Q are reduced to power law behavior, which is a very special case, and tapered exponential has long been advocated (Main and Burton, 1984; Kagan, 1994). By inspection of (12) it can be said that interevent-times exponents are independent in contrast to interevent-distances and seismic-moment exponents, which are always related. Note that while p should be positive so that a decay in events number follows increasing interevent times, b and d are more complex. Aki (1981) stated two scenarios for faults: linear objects filling a surface ($1 \leq d < 2$), or planar objects filling a volume ($2 \leq d < 3$).

Working on disordered materials Carpinteri and Chiaia (1997) suggested two scenarios in fatigue cycles, a loading process defined over lacunar (Cantor-like) sets where progressive void-appearance speeds-up failure by stress concentration, and a release process defined over invasive (Koch-like) sets where progressive detail-appearance speeds-up dissipation by surface-energy build-up. As seen in Figure 2 there is ample space for those scenarios depending on γ values. For instance, if $\gamma = -1$ then invasive sets with dimension $d < 1$ support moment distributions as long as $b \leq 1/3$. On the contrary lacunar sets occur for $b > 1/3$, and values of $\gamma = -2$ are always associated with lacunar sets, as long as $b > 0$.

Finally, a consideration is to be made regarding fractal dimension. In this case the calculated exponents corresponds to bidimensional box-counting dimension d_{BC}, which is an upper limit for Hausdorff dimension d_{H} (Ott, 2002), therefore $d_{\mathrm{H}} \lesssim d_{\mathrm{BC}}$.

https://doi.org/10.5194/egusphere-2026-3399
Preprint. Discussion started: 19 June 2026

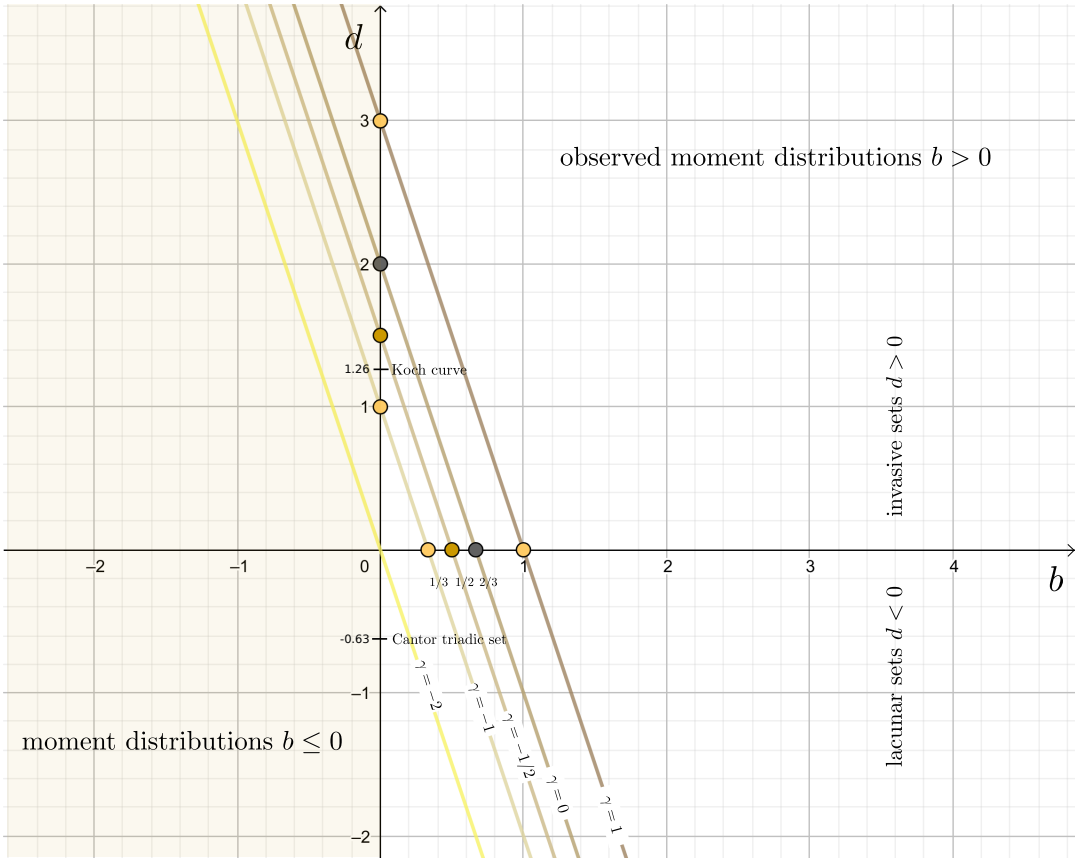

Figure 2. Scaling laws representing the relationship between b and d for various values of γ. Admissible values for b are positive, while d values can be positive (invasive sets) or negative (lacunar sets). Laws with $\gamma \leq -2$ always represent lacunar sets for b positive, laws with $-2 < \gamma$ represent lacunar or invasive sets depending on different values of b. Fractal dimensions for Koch curve and Cantor triadic set are shown as reference.

3 Sismotectonics and data

3.1 Southern Andes tectonic framework

As shown in Figure 3a the Nazca plate advances at 68 $\mathrm{mm\,y^{-1}}$ (Norabuena et al., 1998) in a N76E direction (Angermann et al., 1999) with respect to South America, forming a convergent contact. The trace of convergence (trench) is roughly aligned NS at the greater bathymetric depths. Under the continent, the northern subducting plate segment shows a simple (planar) but abrupt (high angle) morphology up until 33°S (Contreras-Reyes et al., 2012), correlating with a tectonic erosive regime along the overriding plate base. The southern segment shows a flattened subduction plate and a tectonic accretionary border that reaches up until 45°S where an erosive regime develops again. Further south, the Pacific Plate subduces South America at 18 $\mathrm{mm\ y^{-1}}$ under accretionary conditions not fully understood yet (Ranero et al., 2006). The volcanic arc (mostly) follows

https://doi.org/10.5194/egusphere-2026-3399
Preprint. Discussion started: 19 June 2026

the aforementioned tectonic regimes with active volcanoes distributed along the Andes with a sharp gap between 30 and 35°S (Ranero et al., 2006). From 2001 onwards various earthquakes with magnitudes greater than 7.0 have been recorded. Northern notable earthquakes are the 2005 Mw 7.8 Tarapacá earthquake, the 2007 Mw 7.8 Tocopilla earthquake, the 2007 Mw 7.7 Iquique earthquake and the great 2014 Mw 8.2 Iquique earthquake. Central South Andes has not presented earthquakes
235 greater than 6 after 2001, but extensive swarms have been recorded. Southern notable earthquake are 2001 Mw 7.0 Papudo earthquake, the great 2010 Mw 8.8 Maule earthquake, the 2011 Mw 7.1 Arauco earthquake, the great 2015 Mw 8.3 Illapel earthquake and the 2016 Mw 7.6 Chiloé earthquake. A thorough description of these events can be found in Ruiz and Madariaga (2018).

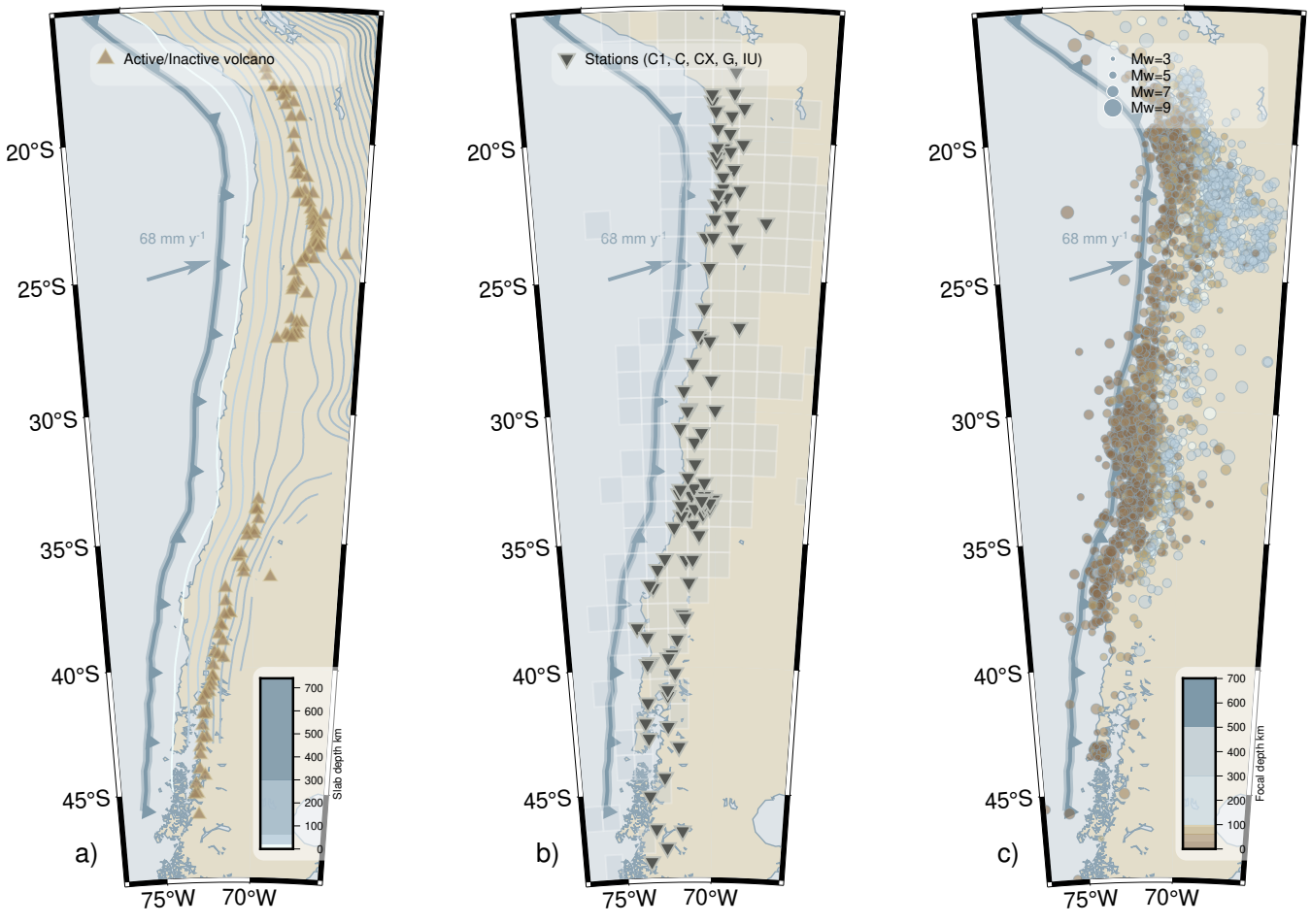

Figure 3. Tectonic, network and earthquake point-catalog context. Left a) plane view of western South America. The subduction trace (trench) is roughly axial to coast line. The Nazca plate advances at 68 mm y^{-1} long-term velocity. A volcanic arc appears parallel to coastline with a remarkable gap correlated with a flatter subduction interface (colored isobath lines). Center b) The seismic network being operated, also a grid with cells covering the region of interest. Right c) Seismicity during 2015-2017 period as published by (Derode et al., 2019).

https://doi.org/10.5194/egusphere-2026-3399
Preprint. Discussion started: 19 June 2026

3.2 Seismic catalog

Figure 3b shows the station network managed by the Plate Boundary Observatory (IPOC), Geoscope, the Global Seismograph Network (GSN) and the Chilean National Seismological Center (CSN). A variety of instruments compose the network. Barrientos (2018) reports the use of modern broadband and accelerometers distributed across the western South Andes border. Thus, there is spatial covering homogeneity but heterogeneous instrumental capacity. In Figure 3c the earthquake point-catalog used in this study is shown, where 6274 earthquakes were detected and analyzed with FMNEAR method (Delouis, 2014) from January 1st, 2015 until December 31, 2017. This method uses fast waveform modeling and has the ability to obtain joint hypocentral localizations and moment tensor, this way a very coherent catalog with precise source position, timing and seismic moment is obtained. In this sense, FMNEAR catalog is a robust and low dispersion experimental dataset. Its short time period is compensated by the high seismic rate and wide moment range observed in southern Andes. Earthquake hypocenters with shallow depth near the trench represent ca. 60% of the catalog whereas 30% are intermediate-depth events (> 70 km), occurring mostly north of 25°S latitude, with prominence between 19 and 23°S. Maximum estimated earthquake depth is 390 km while magnitudes range between Mw 1.7 and 7.8, see Derode et al. (2019) for further details.

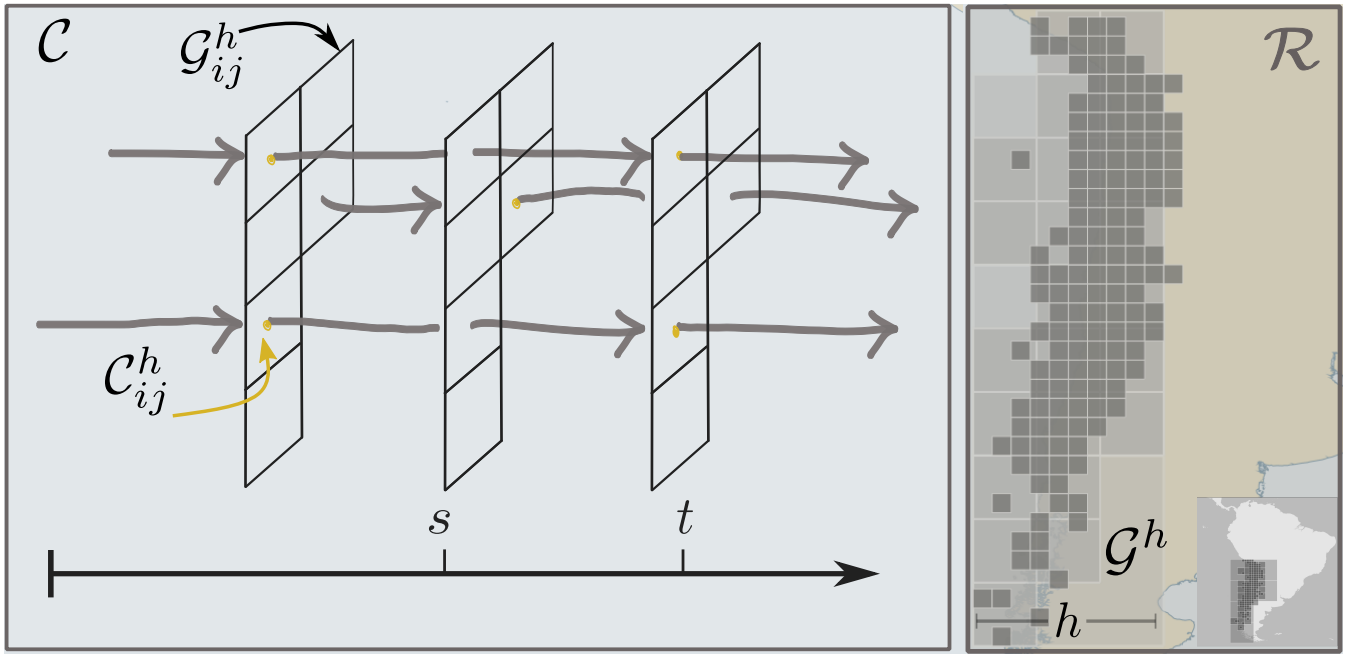

Figure 4. Earthquake point-catalog sketch and gridding-technique. An earthquake point-catalog might be intersected with a grid $\mathcal{G}^h$ covering a region $\mathcal{R}$. An evolution process marked at specific points in time s and t where earthquakes occur is induced, thereby creating a subcatalog $\mathcal{C}_{ij}^h$ for every cell $\mathcal{G}_{ij}^h$, $i, j = 1, 2, \ldots$, within the grid. As different proper scales h are explored, the process precise description changes.

https://doi.org/10.5194/egusphere-2026-3399
Preprint. Discussion started: 19 June 2026

4 Methods

4.1 Gridding and box-counting

The main data analysis tool is the gridding and box-counting technique (Feder, 2013) as shown in Figure 4, right panel. The region $\mathcal{R}$ is covered by a bidimensional grid $\mathcal{G}^h$ composed of cells $\mathcal{G}^h_{ij}$, with proper-length h, where $i, j = 1, 2, \ldots$ are positional indices. The intersection of an earthquake point-catalog $\mathcal{C}$ with $\mathcal{G}^h$ generates subcatalogs $\mathcal{C}^h_{ij}$ composed of all events within the cell $\mathcal{G}^h_{ij}$ as illustrated in Figure 4, left panel. We interpret these subcatalogs as sample paths of a punctuated random-field process portraying a deformation field, with earthquakes acting as points scattered at distances always shorter than h within $\mathcal{G}^h_{ij}$. A key observation is that grid cells at the scale h act as a restriction over the random-field process and its random variables, as the cell proper-length h becomes an upper bound for the interevent distance distribution, this threshold sampling implies a mild declusterization (Janićević et al., 2016). A second key observation concerns the temporal seismic-sequence ordering, as a mainshock and its foreshock-aftershock sequence might be placed on different sample paths (subcatalogs) as we go to smaller or larger cell proper-lengths, it follows that earthquake denominations become local and scale relative.

To fulfill the first similarity hypothesis, a cutoff must be imposed on every event in every subcatalog. We built the cell proper-lengths matching the typical earthquake source radius $r^3 = \frac{7}{16}\frac{Mo}{\Delta\sigma}$ from Madariaga (2020) and we selected only those events with estimated radius smaller than cell proper-length h, under these conditions Π_u is always small. Subcatalogs with 4 events or more are retained, although 3 points are required by most unbiased maximum-likelihood estimators and 2 points are required by unbiased variance estimators.

4.2 Statistical tools

Our random path interpretation across cells is based on a *locally homogeneous* idea introduced by Kolmogórov (1941b), that is distributions on the grid cells $\mathcal{G}^h_{ij}$ for a given proper-length h are independent on the initial time and they depend only on differences along the paths (time stationarity) and across the cells (space homogeneity) this conditions allow us to obtain meaningful experimental histograms for random variables like τ, ℓ and Mo for a given proper-length scale h. For each cell, after the subcatalogs are obtained, maximum interevent times, maximum interevent distances and maximum seismic-moment are calculated, and these new random variables, by dimensional considerations, also follow the scaling relations in equations (11) and (12) thus they represent valid statistical estimators. The use of maximum values for the cell random variables is also a dimensional reduction operator and acts like the majority rule in spin ± 1 systems (Wilson, 1979), where passage from smaller to larger cells is accomplished by selecting the most frequent spin. This is another justification for the coarse-graining renormalization terminology used. This choice of maximal bounds avoids the use of binned density histograms, therefore we obtain cumulative experimental histograms which are more stable than density statistics known as source of problems in power law data (Virkar and Clauset, 2014) and also smears a known bias when fitting logarithmic data with least squares (Goldstein et al., 2004).

The scaling function Φ^* in Eq. (11) is unknown, and supposing a power law translate the problem to a careful exponent estimation using constrained optimization fit (Branch et al., 1999). We understand this collapse procedure as fixed point iterations

https://doi.org/10.5194/egusphere-2026-3399
Preprint. Discussion started: 19 June 2026

—using the renormalization group— in search for the special situation where all data fall-in a single curve that represents a stable point in the parametric space, see Houdayer and Hartmann (2004). From a seed around stable exponents, 2500 iterations are produced each time sampling 25% of the data, so that mean values with 2σ reverse bootstrap percentile intervals (Diaconis and Efron, 1983; Efron and Tibshirani, 1994) are reported (see Table 3).

5 Results

First order statistics are shown in Table 2. We used 6 grids, having cell (edge) proper-lengths between 3–1000 km. The grid with cells ca. 100 km proper-length is shown in Figure 3 b, see links to maps and tabulated statistics in the Open Research section. The number of cells decrease from 4848 at proper-length 3 km to 4 at proper-length 1000 km, representing a lacunar fractal with dimension 1.24. Including the lower bound on number of events, cells decrease from 429 to 4.

Table 2. Grid characteristics used in the study, see Figure 3b. For a given proper-length h a set of cells $\mathcal{G}_{ij}^h$, $i,j = 1,2,\ldots$ is laid out over a region $\mathcal{R}$. A set of subcatalogs $\mathcal{C}_{ij}^h$ is created, one for each cell. We interpret them as random paths, see Figure 4. Random variables over those paths are τ, ℓ and Mo. We show basic upper-lower bounds for maximum estimators over the path ensemble indexed by h.

$\ell/\sqrt{2} \lesssim h$ m	cell count		interevent times τ μs		scalar moment Mo N m		interevent distances ℓ m	
	$i \geq 1$	≥ 4	upper	lower	upper	lower	upper	lower
$3.\bar{3} \cdot 10^3$	4848	105	$9.24 \cdot 10^{13}$	$2.16 \cdot 10^{11}$	$3.98 \cdot 10^{16}$	$7.94 \cdot 10^{13}$	$4.40 \cdot 10^3$	$1.45 \cdot 10^3$
$1.0 \cdot 10^4$	2498	429	$9.38 \cdot 10^{13}$	$1.73 \cdot 10^{11}$	$1.26 \cdot 10^{18}$	$7.94 \cdot 10^{13}$	$1.37 \cdot 10^4$	$3.08 \cdot 10^3$
$3.\bar{3} \cdot 10^4$	688	312	$9.43 \cdot 10^{13}$	$6.14 \cdot 10^{12}$	$2.82 \cdot 10^{19}$	$7.94 \cdot 10^{13}$	$4.78 \cdot 10^4$	$1.12 \cdot 10^4$
$1.0 \cdot 10^5$	154	88	$9.46 \cdot 10^{13}$	$2.76 \cdot 10^{13}$	$6.31 \cdot 10^{20}$	$6.31 \cdot 10^{14}$	$1.48 \cdot 10^5$	$3.35 \cdot 10^4$
$3.\bar{3} \cdot 10^5$	29	20	$9.46 \cdot 10^{13}$	$4.86 \cdot 10^{13}$	$6.31 \cdot 10^{20}$	$2.00 \cdot 10^{16}$	$4.83 \cdot 10^5$	$6.70 \cdot 10^4$
$1.0 \cdot 10^6$	4	4	$9.46 \cdot 10^{13}$	$8.75 \cdot 10^{13}$	$6.31 \cdot 10^{20}$	$1.00 \cdot 10^{19}$	$1.16 \cdot 10^6$	$6.59 \cdot 10^5$

The grid with proper-length 3.3 km, containing events with interevent distances ℓ no greater that 4.7 km, show maximum interevent times from $2.16 \cdot 10^{11}$ s to $9.24 \cdot 10^{13}$ s, a range from days to years. The grid with cell proper-length 10 km shows a similar period range. The grid with cell proper-length 33 km show maximum interevent times range from $6.14 \cdot 10^{12}$ s to $9.43 \cdot 10^{13}$ s, weeks to years. Grids with proper-lengths 100, 333 and 1000 km have lower and upper maximum interevent times in the years range. Scalar seismic moment shows the effect of the first similarity hypothesis, as earthquake sizes (in terms of source radius) shows a cutoff depending on cell proper-length, therefore the seismic-moment ranges are bounded based on geometric and physical conditions within a grid. Interevent distances shows the restrictive effect of the threshold sampling induced by grid cell proper-length, it happens that $\ell/\sqrt{2} \lesssim h$.

Figure 5 show cell maximum dimensionless interevent frequency Π_T versus dimensionless event number Π. Different symbols represent cell proper-length as shown in Table 2. Symbol sizes represent cell maximum magnitudes. Longer interevent

https://doi.org/10.5194/egusphere-2026-3399
Preprint. Discussion started: 19 June 2026

times have dimensionless parameter $\Pi_T \simeq 1$, shorter interevent times have $\Pi_T \to \infty$. The longer observed times with $\Pi_T \simeq 1$ happens always at $h \simeq 1000$ km —star symbols— and those larger cells contain larger number of events. Then a general trend of shorter cell maximum interevent frequency is seen as cell proper-length diminishes —square and pentagon symbols. Note also the natural decrease in cell event number because of shorter cell proper-length with very large Π_T. Big symbols indicating larger cell maximum magnitudes are associated with large Π values, a signature of aftershock clustering, but there are considerable fluctuations. In general, a very skewed distribution emerges, with appreciable dispersion.

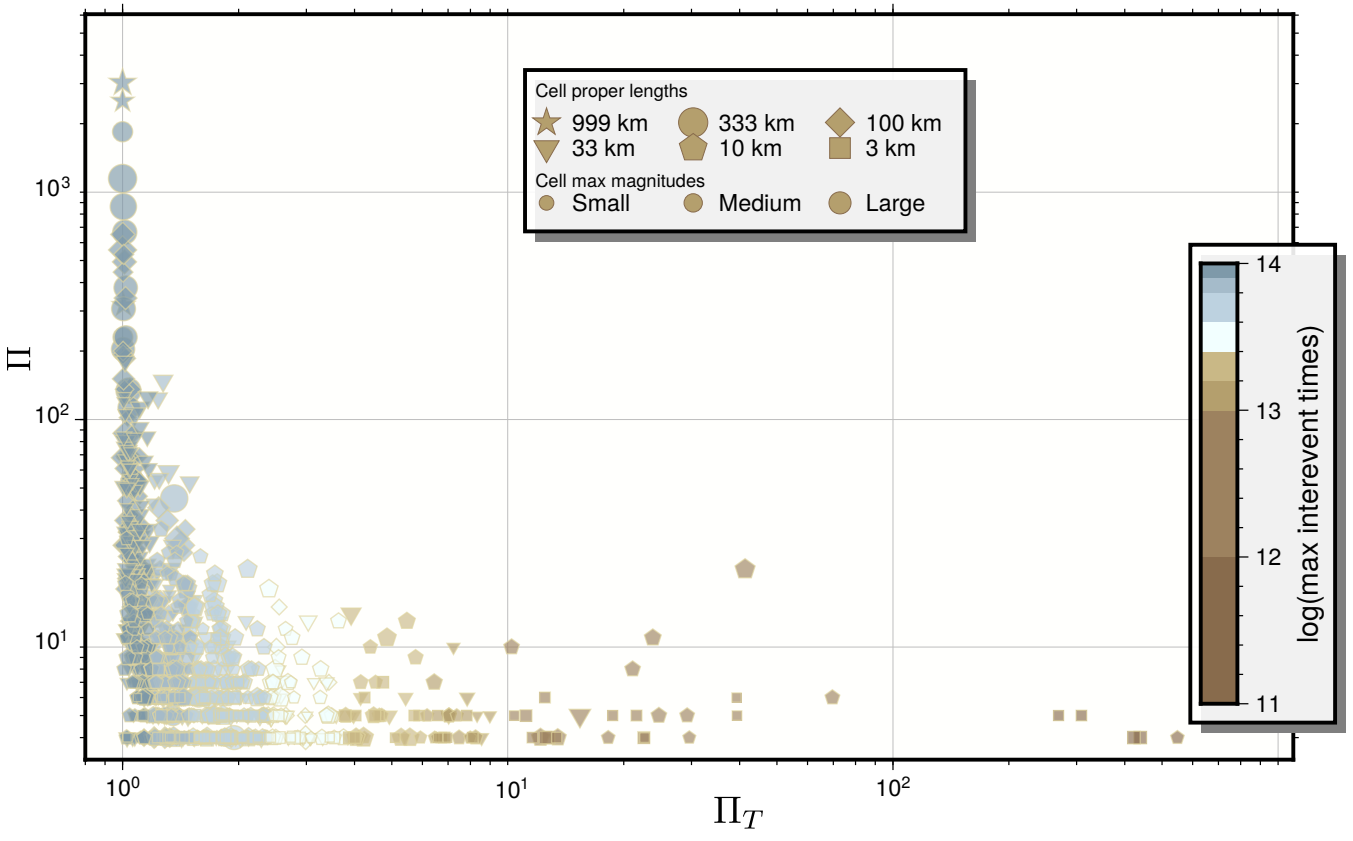

Figure 5. Statistical properties of cell maximum frequency Π_T. Different symbols represent cell proper-length as shown in Table 2. Symbol sizes represent cell maximum magnitudes. For each cell $\mathcal{G}_{ij}^h$, $i, j = 1, 2, \ldots$ at every cell proper-length h the cell maximum interevent frequency Π_T versus the cell dimensionless event number Π is shown. See text for description.

Figure 6 show cell maximum dimensionless seismic moment Π_{Mo} versus event number Π. Different symbols represent cell proper-length as shown in Table 2. Symbol sizes represent cell maximum magnitudes. Cells with longer proper-length —star symbols— have large event number Π but they do not have the larger cell maximum dimensionless seismic moment Π_{Mo}. Some large cells —with circle symbols— have very small cell maximum dimensionless seismic moment Π_{Mo} despite large cell moment magnitude (bigger symbol sizes). In general, a very skewed distribution emerges, with appreciable dispersion.

https://doi.org/10.5194/egusphere-2026-3399
Preprint. Discussion started: 19 June 2026

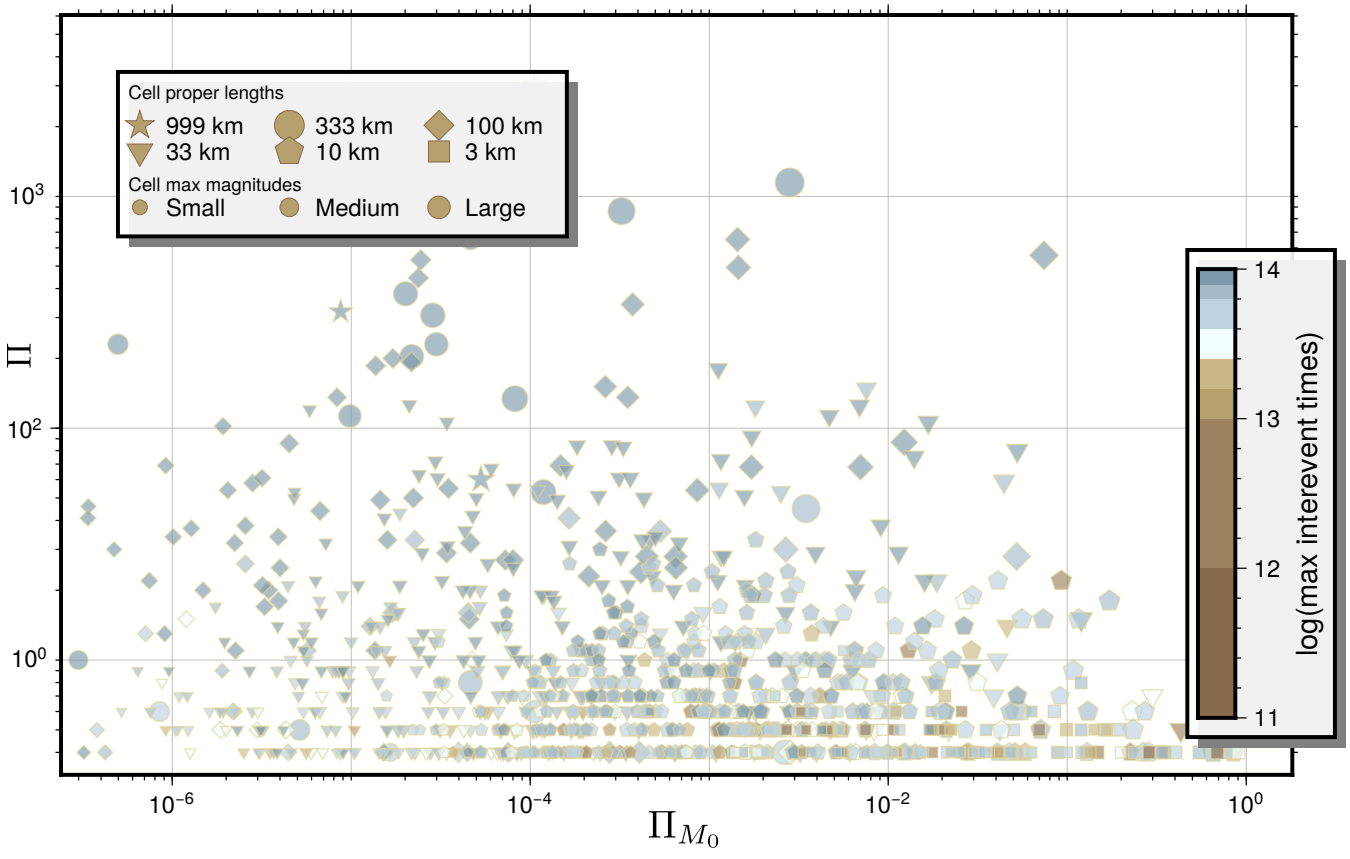

Figure 6. Statistical properties of cell maximum dimensionless seismic moment Π_{Mo}. Different symbols represent cell proper-length as shown in Table 2. Symbol sizes represent cell maximum magnitudes. For each cell in $\mathcal{G}_{ij}^{h}$, $i, j = 1, 2, \ldots$ at every cell proper-length h the cell maximum dimensionless seismic moment Π_{Mo} versus the cell dimensionless event number Π is shown. See text for description.

Figure 7 show cell maximum interevent wavenumber Π_H versus Π. Different symbols represent cell proper-length as shown in Table 2. Symbol sizes represent cell maximum magnitudes. Cells with longer proper-lengths —star symbols— have the smaller dimensionless interevent wavenumber and cells with shorter proper-length —square symbols— have larger dimensionless interevent wavenumber. Event number Π tends to be larger for smaller Π_H but there is mixed behavior as $\Pi_H \to \infty$. The gridding technique restrictive action is seen as cell maximum interevent wavenumber tends to be clustered around a fixed proper-cell length h, so that $\ell/\sqrt{2} \lesssim h$. In general, very skewed distributions emerge as well.

In Figure 8 a plot sequence illustrating renormalized seismic-moment release-rate Π_Q^* versus renormalized event number Π^* curves is shown. Colors represent maximum interevent times, symbols represent cell proper-lengths and symbol sizes maximum magnitudes. Coefficients used to scale dimensionless variables are indicated in the legend. Each plot shows Φ^* as a function of $\gamma = -3, -1, 0, 1, 2, 3$. Upper-left plot, with $\gamma = -3$, shows curve splitting and Φ^* multivaluedness. Judging by the colors, maximum interevent times are scattered with no evident pattern. Cells with large maximum magnitudes are placed at

https://doi.org/10.5194/egusphere-2026-3399
Preprint. Discussion started: 19 June 2026

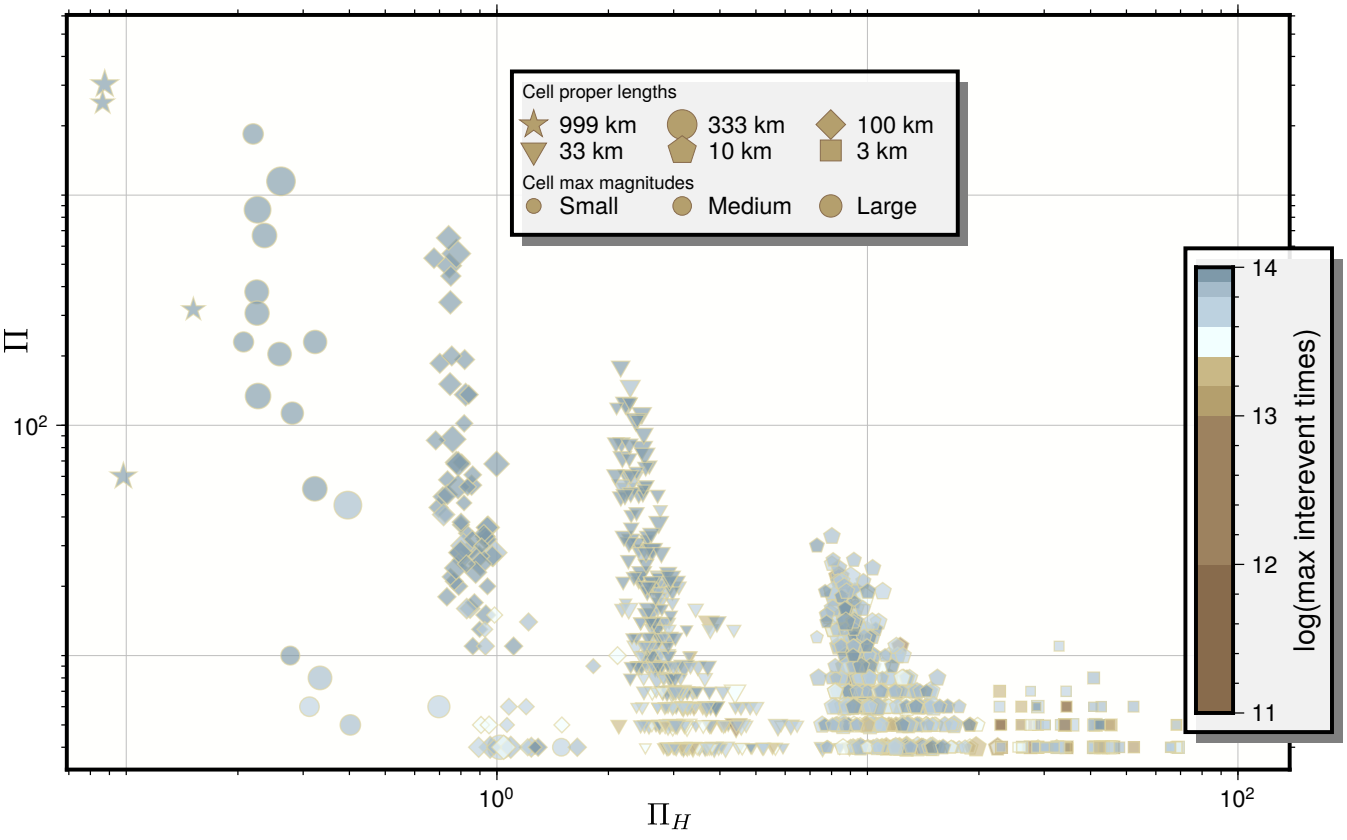

Figure 7. Statistical properties of cell maximum interevent wavenumber Π_H. Different symbols represent cell proper-length as shown in Table 2. Symbol sizes represent cell maximum magnitudes. For each cell in $\mathcal{G}_{ij}^h$, $i,j = 1,2,\ldots$ at every cell proper-length h the cell maximum dimensionless interevent wavenumber Π_H versus the cell dimensionless event number Π is shown. See text for description.

small Π_Q^* values with long h. Although same proper-length cells tend to be grouped together, there is increasing dispersion as h decreases. No unique scaling function Φ^* can possible describe this situation. As γ increases all cells tend to a single curve, diminishing overall dispersion. We interpret this process as a renormalized fixed point iteration flow (McComb, 2003).

In Table 3 a comparison from theoretical models and studies with similar scalings laws are shown together. The row labeled theory refer to branching model as explained in Kagan (1994), we use Eq. (12) to fill-in the corresponding values with $\beta = -1/2$ and a fractal surface. Kossobokov and Mazhkenov (1994) propose a magnitude-distance analysis, therefore $\alpha = -1$ to give $p = 0$ (same with α_Q) and also $\beta_Q = 0$, $\gamma_Q = 3$ so that only β and γ are fitted with observations from Southern California between 1980 and 1987. Bak et al. (2002) uses a time-magnitude-distance analysis with a very particular *ansatz* with $\alpha_Q = 0$, $\beta = 0$ and $\gamma = -2$, so that α, β_Q and γ_Q are fitted with observations from California between 1984 and 2000. We can not faithfully compare these data, given the evident differences in methodology, but general observations can be made. It can be said that our results are more general, because times, distances and seismic-moment have one pair of exponents, an idea first explored by Bak et al. (2002). Our calculations show exponents obtained after the proposed collapsing process

https://doi.org/10.5194/egusphere-2026-3399
Preprint. Discussion started: 19 June 2026

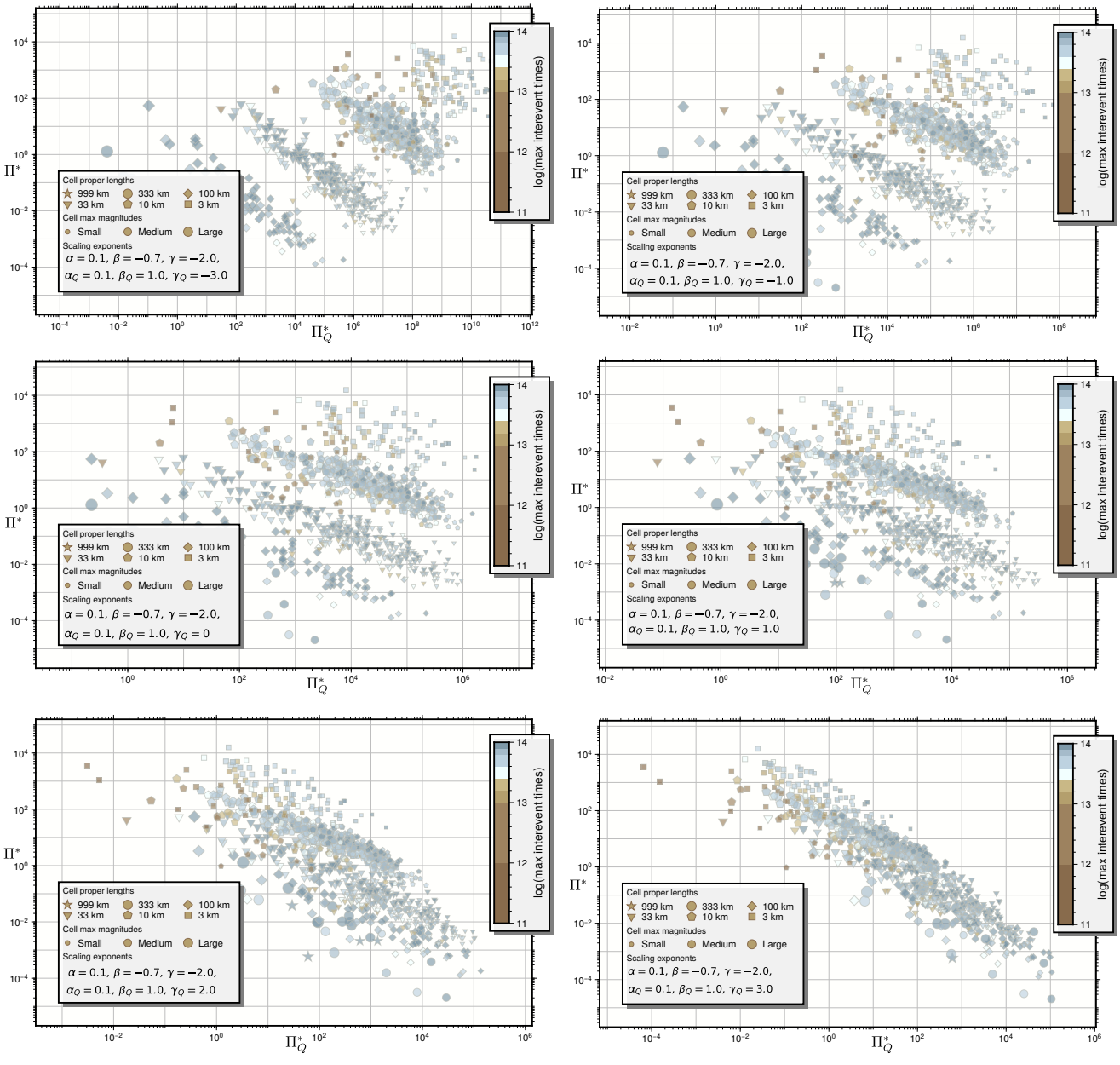

Figure 8. Collapsing process. Plot sequence illustrating cell maximum Π_Q^* versus cell Π^* curves collapsing as a function of $\gamma_Q = -3, -1, 0, 1, 2, 3$ as indicated in the legend within. Minimum dispersion state might be clearly observed as γ_Q grows, see Figure 9 where a final state has been reached. This evolution process might be interpreted as a renormalized fixed point iteration flow (McComb, 2003). Referential seismogenic thickness $H = 1.00 \cdot 10^5$ m, observation period $T = 9.46 \cdot 10^7$ s (3 years) stress-drop $\Delta\sigma = 4.00 \cdot 10^6$ Pa, and seismic-moment release-rate $Q = 1.50 \cdot 10^{12}$ W.

https://doi.org/10.5194/egusphere-2026-3399
Preprint. Discussion started: 19 June 2026

Table 3. Scaling exponents as seen in Figure 9, referential value from theory and other studies with similar scaling laws are shown as reference, see text for discussion.

	α	β	γ	α_Q	β_Q	γ_Q
theory†	-1.00	$-\frac{1}{2}$	-1.50	-1.00	$+0.00$	$+3.00$
Southern California•	-1.00	$-0.59^{0.02}_{0.02}$	$-2.26^{0.04}_{0.04}$	-1.00	$+0.00$	$+3.00$
California‡	$+0.00^{0.20}_{0.20}$	$+0.00$	-2.00	$+0.00$	$+0.70^{0.20}_{0.20}$	$+2.20^{0.20}_{0.20}$
collapsed¶	$-0.5998^{0.0019}_{0.0018}$	-0.6900	$-1.3949^{0.0012}_{0.0010}$	$-0.1002^{0.0019}_{0.0013}$	$+0.8900$	$+3.8947^{0.0016}_{0.0011}$

† Values in: Kagan (1994), $b = b_{\mathrm{GR}} = 3/4$ and γ a fractal surface
• Values in: Kossobokov and Mazhkenov (1994), $b_{\mathrm{GR}} = 0.89$, $d = 1.51$
‡ Values in: Bak et al. (2002), $p \simeq 1$, $p_Q = 1$, $b_Q = b_{\mathrm{GR}} \simeq 1$, $d_Q = 1.2$
¶ Stress-drop $\Delta\sigma = 4.00 \cdot 10^6$ Pa, seismic-moment release-rate $Q = 1.50 \cdot 10^{12}$ W

with bootstrapped lower-upper indices for left-right statistical deviations. Seismic-moment β and β_Q exponents do not display appreciable variance to be reported, which is consistent with findings in Kagan (2002). Likewise α, α_Q, γ and γ_Q also have small variability and all of them show a mild statistical skewness, that is, a slight difference between left and right deviations, though they are very stable. If the comparison is valid, there is a positive bias in α_Q and γ_Q with respect to theory and studies in California, probably because of maximum statistics used here and differences in tectonic environment.

In Figure 9 a final state is shown. A single function $\Pi^* = \Phi^*(\Pi_Q^*)$ is displayed. There is considerable scatter, but a general trend where data at all involved scales collapse across 11 orders of magnitude. In this particular case —averaged over a large geographical extent fitting data across Southern Andes— a single scaling function Φ^* with power-law shape $\Pi^* \simeq {\Pi_Q^*}^{\epsilon}$, $\epsilon = -0.835$ might be proposed, but we do not rule out a tapered or other scaling laws, see Siegel et al. (2022) and Discussion below. Coefficients used to renormalize n and Q are indicated in the legend and also in Table 3. Considering the large geographic extent, scaling exponents should be taken as averaged values, as fluctuations are present when considering each grid alone. These exponents are not material parameters, they depend on the problem at hand, including its boundary conditions, so that specific places with different values are perfectly possible. Note that cells with large maximum seismic moment, shown as big symbols, do not align with dimensionless seismic moment release-rate, which is critical in seismic risk analysis, this is the most important similarity property, because after the proposed renormalization, cells very far away in terms of interevent times, interevent distances or seismic moment might end-up very close in this plot.

6 Discussion

6.1 Similarity hypothesis

Considering the first similarity hypothesis about small-strain condition over Π_u, i.e. the condition on fault-displacements much smaller than ℓ, it might be said that it allows a statistical treatment across cells within a grid, i.e. no seismic event can grow

https://doi.org/10.5194/egusphere-2026-3399
Preprint. Discussion started: 19 June 2026

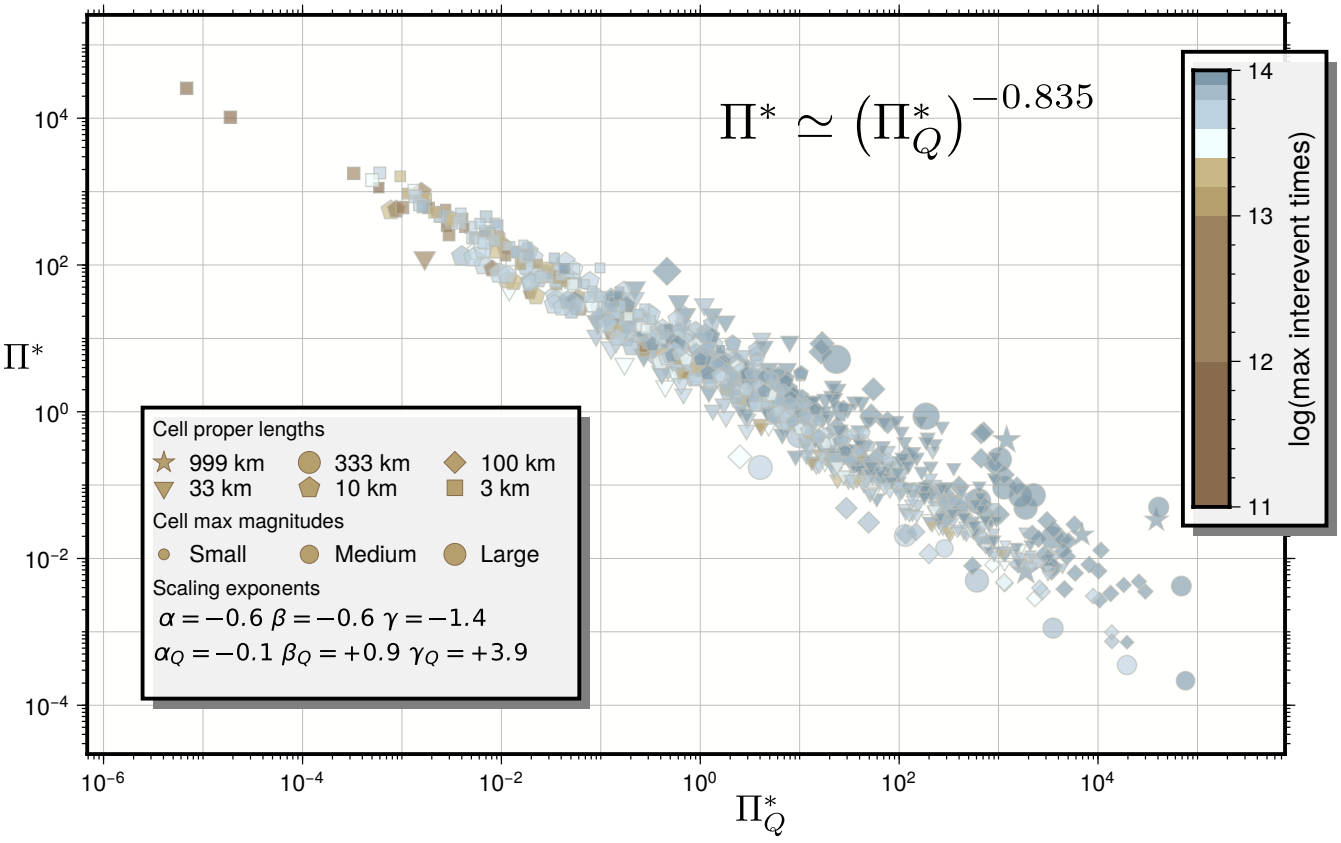

Figure 9. Collapsed scaling situation. Cell maximum renormalized seismic moment release-rate Π_Q^* versus cell renormalized event number Π^* collapsed state, note the strong overlapping in terms of cell proper-lengths and cell maximum interevent times, which is critical in earthquake hazard estimation. A power-law behaviour $\Phi^* \simeq {\Pi_Q^*}^{\epsilon}$ could be proposed with overall exponent $\epsilon = -0.835$ across 11 orders of magnitude. Exponents as shown in Table 3 also depicted in the legend within. Referential seismogenic thickness $H = 1.00 \cdot 10^5$ m, observation period $T = 9.46 \cdot 10^7$ s (3 years) stress-drop $\Delta\sigma = 4.00 \cdot 10^6$ Pa, and seismic-moment release-rate $Q = 1.50 \cdot 10^{12}$ W.

outside cell boundaries, therefore the cell seismic moment histograms do not consider events excessively large with respect to the cell proper-length and also cell interevent distance histograms do not take into account dissimilar pairs. Further analysis will require a catalog with variables regarding processes with smaller scales, that is, the information from the physics at the seismic source. Considering the second similarity hypothesis, the large dynamical range achieved by the renormalized parameters with a single set of exponents fitting a reasonably well behaved function Φ^* suggest that it is physically sound. Other earthquake point-catalogs, with wider observational data range should be studied to further confirm this hypothesis. Regarding the third hypothesis, as suggested by Benzi et al. (2022), a steady seismic-moment release-rate is a variable affecting interevent time distributions, to further explore it a catalog describing a wider spectrum of phenomena is needed (Beroza and Ide, 2011; Ide et al., 2007; Ito et al., 2007). We must remark that a constant Q value means that a constant injected energy fraction is used in seismicity generation, in this regard the seismic-moment released by slow mechanisms —Kato et al. (2012); Uchida and

https://doi.org/10.5194/egusphere-2026-3399
Preprint. Discussion started: 19 June 2026

Matsuzawa (2013) in Japan and Ruiz et al. (2014); Holtkamp et al. (2011); Klein et al. (2018); Socquet et al. (2017) in Southern Andes— should be explored in the future.

6.2 Magnitude cutoff

The completeness of an earthquake point-catalog, that is the lower magnitude cutoff assuring a Gutenberg-Richter law, is related to the dimensionless moment Π_{Mo}. It is an additional parameter not considered in the original frequency-magnitude formulation, much like the upper magnitude cutoff used in maximum-likelihood statistical estimator of b_{GR}. To estimate the lower cutoff magnitude, various criteria have been proposed (Mignan and Woessner, 2012) and our collapse procedure can be used as an aditional criteria and its statistical properties should be studied in future works.

6.3 Homogeneity and isotropy

Other earthquake point-catalog characteristics that should be explored, in the proposed context, are grid translation and rotation. As our notion of statistical homogeneity operates within grid cells, global statistical homogeneity is not explored. Time features like intermittency and quiescence, spatial characteristics like clustering and geological properties such as fault strike populations should provide new constrains on the random field processes analyzed. As our grid analysis is bidimensional, depth variations are currently lost. Future analysis should deal with these shortcomings.

6.4 Seismic cycle and hazard

The scaling found, fitting data across the southern Andes, suggest that tectonic segments with large quiescent gaps follow the same scaling shown in Figure 9, therefore near and distant segments are correlated, thus inferences using isolated data within gaps are inherently biased. As the gridding technique comprehensively covers the observable interevent distances, times and seismic moment distributions from all scales, our results are stable catalog properties, thus hazard estimators might profit from the correlations just showed.

6.5 Cascade of energy

Kagan (1992) suggested turbulence as a model for seismicity given that various phenomena like stochasticity, power-law behaviour, and large number of degrees-of-freedom are common to both phenomena. For a given grid $\mathcal{G}^h$, as the first similarity hypothesis states, there is no fault growth across cells, which raises a seismic-moment transfer question. A simple candidate is a mechanism involving passage along grids, that is from one proper-length to another. As our theoretical analysis does not include an explicit dissipation mechanism, a lossless seismic-moment transfer process appears naturally. This scenario is analog to the cascade mechanism in turbulence (Batchelor, 1947) where vortices are created (or destroyed) without energy loss as long as the fluid is confined in an *inertial range* where vortices are small compared to the fluid proper-length scale. This range is a region delimited by two length boundaries. A lower length acting as an upper limit for viscous dissipation processes and an upper length acting as a lower limit for forcing processes. In between, the energy transfer is characterized by a viscous-

https://doi.org/10.5194/egusphere-2026-3399
Preprint. Discussion started: 19 June 2026

free energy rate dissipation spectra decaying as $\ell^{-5/3}$ (Kolmogórov, 1941a; Frisch, 1995). If the analogy stands, there must be a physical proper-length λ where earthquake source micro-processes taking place at shorter lengths might be considered stationary, so that lossless seismic-moment transfer take place when going up to lengths longer than λ. In other words, as long as the first similarity hypothesis over Π_u is fulfilled, no seismic-moment is lost when passing from one proper-length to another, i.e. along grids. Likewise, there must be a proper-length where seismic-moment transfer processes between grids ceases to be dissipation free. A larger length $\Lambda = \sqrt[3]{Q/(\Delta\sigma T^{-1})} \simeq 30$ km is a candidate, but further studies are needed.

6.6 Tectonics

The renormalized event number distribution scales with $p = 0.4$, $b_{\mathrm{GR}} = 1.035$, and $d_{\mathrm{BC}} = -1.465$, that is a maximum seismic moment release distribution with decaying power law, non-exponential maximum interevent times and lacunar-set support. By the time of the 1995 $Mw\,8.5$ Antofagasta earthquake, Sobiesiak (2000) reported $b_{\mathrm{GR}} = 0.73$ over the fault plane with peaks at 0.54 and 1.08. On a similar region Pastén and Comte (2014) gave a multifractal series converging to $d_\infty = 1.45$, so our estimates are higher on average. A global survey by Nishikawa and Ide (2014) reports b_{GR} values at six sections located between $19.8°$S and $34.2°$S latitude. Peaks range from $b_{\mathrm{GR}} = 0.79$ to 0.94 with a decreasing north-south trend. These values are in good accord with our findings. Finally Poulos et al. (2019) gives values between $b_{\mathrm{BR}} = 0.87$ and $b_{\mathrm{GR}} = 1.04$ for their zones 1 and 5, which are also consistent with our findings. Therefore, as indicated by Carpinteri and Chiaia (1997), the 2015-2017 Southern Andes were in a loading situation.

7 Conclusions

Several conclusions can be drawn from the study. First, the renormalized parameters are completely determined by a set of scaling equations (12) involving exponents only. These equations represent scaling laws for interevent times, interevent distances and seismic-moment. These findings come from two fundamental symmetries, which generate invariants, one of them of a general nature and the other particular to the problem. One invariant emerges after the application of the group of transformations defining change from one system of units to another and the other emerges after the action of the renormalization group of transformations, thus exponents and scaling functions characterize regions with its particular settings, they are not universal.

Second, the particular conditions of each problem are established by the asymptotic behavior of the physical laws when varying the governing parameters of the system. If the system ceases to depend on a governing parameter when very large or very small values are considered, we speak of complete similarity and if the behavior continues to depend on the governing parameter, as it goes to very small or very large values, we speak of incomplete similarity. In the southern Andes, we have shown evidence that both behaviors are present in the seismic catalog between 2015 and 2017. The complete similarity conditions take us to a gridding methodology that we interpret in terms of sample paths. Passing from one grid to another is accomplished by a coarse graining maximum operator. Incomplete similarity conditions are interpreted as well known long-range correlations.

https://doi.org/10.5194/egusphere-2026-3399
Preprint. Discussion started: 19 June 2026

Those conditions define an intermediate asymptotics, which we associate with a bounded seismic-moment transfer mechanism along scales.

Third, the role of the observation period T and its influence on the inferences might be assessed in terms of the larger scale linked with the seismic-moment transfer mechanism. The upper boundary length growths with the cubic root of the observation period, therefore various decades are needed to obtain an idea of the seismic generation process at the tectonic scale.

Code availability.

Data availability. Processed catalog data in spreadsheet format as well as shapefile vector files available at zenode repository 10.5281/zenodo.8008235.

Code and data availability.

Sample availability.

Video supplement.

Author contributions. PT:Conceptualization, formal analysis, software, writing. CS: formal analysis, validation, writing. RM: Supervision, writing. JC: Supervision, resources, writing.

Competing interests. The authors declare no competing interests

Acknowledgements. PT, RM and JC acknowledge financial support from the Seismic Risk Program (PRS). We thank IPOC collaboration affiliated institutions (German Research Center For Geosciences (GFZ), Germany; GEOSCOPE Program of Institut de Physique du Globe de Paris and C.N.R.S., France; Centro Sismológico Nacional (CSN) Universidad de Chile, Chile; and Universidad Católica del Norte, Chile) GFZ German Research Centre For Geosciences and Institut Des Sciences De L'Univers-Centre National De La Recherche CNRS-INSU (2006); Barrientos (2018) for the seismic network maintenance that made this work possible. We thank Ian Main for its thorough revision,

https://doi.org/10.5194/egusphere-2026-3399
Preprint. Discussion started: 19 June 2026

comments and links to relevant literature. We also thank an anonymous reviewer for his comments as they helped us to clarify very important issues in the initial draft.

Figures were made with GMT (Wessel et al., 2019), pyGMT (Tian et al., 2023) and Inkscape. Gridding technique was implemented with GRASS GIS (Neteler et al., 2012). Catalog analysis were made with Numpy (Harris et al., 2020).

https://doi.org/10.5194/egusphere-2026-3399
Preprint. Discussion started: 19 June 2026

References

Aki, K.: Scaling law of seismic spectrum, Journal of Geophysical Research, 72, 1217–1231, 1967.

Aki, K.: Earthquake mechanism, Tectonophysics, 13, 423–446, 1972.

Aki, K.: A Probabilistic Synthesis of Precursory Phenomena, pp. 566–574, American Geophysical Union (AGU), ISBN 9781118665749, https://doi.org/10.1029/ME004p0566, 1981.

Aki, K.: Scale dependence in earthquake phenomena and its relevance to earthquake prediction, Proceedings of the National Academy of Sciences, 93, 3740–3747, 1996.

Allmann, B. P. and Shearer, P. M.: Global variations of stress drop for moderate to large earthquakes, Journal of Geophysical Research: Solid Earth (1978–2012), 114, 2009.

Angermann, D., Klotz, J., and Reigber, C.: Space-geodetic estimation of the Nazca-South America Euler vector, Earth and Planetary Science Letters, 171, 329–334, 1999.

Bak, P., Christensen, K., Danon, L., and Scanlon, T.: Unified scaling law for earthquakes, Physical Review Letters, 88, 178 501, 2002.

Barenblatt, G. I.: Dimensional analysis, CRC Press, 1987.

Barenblatt, G. I.: Scaling, Self-similarity, and Intermediate Asymptotics: Dimensional Analysis and Intermediate Asymptotics, Cambridge Texts in Applied Mathematics, Cambridge University Press, https://doi.org/10.1017/CBO9781107050242, 1996.

Barenblatt, G. I.: Scaling, Cambridge Texts in Applied Mathematics, Cambridge University Press, https://doi.org/10.1017/CBO9780511814921, 2003.

Barenblatt, G. I.: Flow, Deformation and Fracture: Lectures on Fluid Mechanics and the Mechanics of Deformable Solids for Mathematicians and Physicists, Cambridge Texts in Applied Mathematics, Cambridge University Press, https://doi.org/10.1017/CBO9781139030014, 2014.

Barrientos, S.: The seismic network of Chile, Seismological Research Letters, 89, 467–474, 2018.

Batchelor, G.: Kolmogoroff's theory of locally isotropic turbulence, in: Mathematical Proceedings of the Cambridge Philosophical Society, vol. 43, pp. 533–559, Cambridge University Press, 1947.

Benzi, R., Castaldi, I., Toschi, F., and Trampert, J.: Self-similar properties of avalanche statistics in a simple turbulent model, Philosophical Transactions of the Royal Society A: Mathematical, Physical and Engineering Sciences, 380, 20210 074, https://doi.org/10.1098/rsta.2021.0074, 2022.

Beroza, G. C. and Ide, S.: Slow earthquakes and nonvolcanic tremor, Annual review of Earth and planetary sciences, 39, 271–296, 2011.

Branch, M.-A., Coleman, T., and Li, Y.: A subspace, interior, and conjugate gradient method for large-scale bound-constrained minimization problems, SIAM Journal on Scientific Computing, 21, 1–23, 1999.

Bridgman, P. W.: Dimensional Analysis, Kessinger Publishing, LLC, ISBN 0548597286, 2007.

Camus, P., Arenas, F., Lagos, M., and Romero, A.: Visión histórica de la respuesta a las amenazas naturales en Chile y oportunidades de gestión del riesgo de desastre, Revista de Geografía Norte Grande, pp. 9–20, 2016.

Carpinteri, A. and Chiaia, B.: Multifractal scaling laws in the breaking behaviour of disordered materials, Chaos, Solitons & Fractals, 8, 135–150, 1997.

Christensen, K., Danon, L., Scanlon, T., and Bak, P.: Unified scaling law for earthquakes, Proceedings of the National Academy of Sciences, 99, 2509–2513, 2002.

https://doi.org/10.5194/egusphere-2026-3399
Preprint. Discussion started: 19 June 2026

Cisternas, M., Torrejón, F., and Gorigoitía, N.: Amending and complicating Chile's seismic catalog with the Santiago earthquake of 7 August 1580, Journal of South American Earth Sciences, 33, 102–109, 2012.

Contreras-Reyes, E., Jara, J., Grevemeyer, I., Ruiz, S., and Carrizo, D.: Abrupt change in the dip of the subducting plate beneath north Chile, Nature Geoscience, 5, 342, 2012.

Corral, A.: Local distributions and rate fluctuations in a unified scaling law for earthquakes, Physical Review E, 68, 035 102, 2003.

Corral, A.: Renormalization-group transformations and correlations of seismicity, Physical review letters, 95, 028 501, 2005.

Delouis, B.: FMNEAR: Determination of focal mechanism and first estimate of rupture directivity using near-source records and a linear distribution of point sources, Bulletin of the Seismological Society of America, 104, 1479–1500, 2014.

Derode, B., Delouis, B., and Campos, J.: Systematic Determination of Focal Mechanisms over a Wide Magnitude Range: Insights from the Real-Time FMNEAR Implementation in Chile from 2015 to 2017, Seismological Research Letters, 90, 1285–1295, 2019.

Diaconis, P. and Efron, B.: Computer-intensive methods in statistics, Scientific American, 248, 116–131, 1983.

Efron, B. and Tibshirani, R. J.: An introduction to the bootstrap, CRC press, 1994.

Feder, J.: Fractals, Springer Science & Business Media, 2013.

Frisch, U.: Turbulence: the legacy of A.N. Kolmogorov, Cambridge university press, 1995.

GFZ German Research Centre For Geosciences and Institut Des Sciences De L'Univers-Centre National De La Recherche CNRS-INSU: IPOC Seismic Network, https://doi.org/10.14470/PK615318, 2006.

Godano, C.: A new expression for the earthquake interevent time distribution, Geophysical Journal International, 202, 219–223, 2015.

Goldenfeld, N. D.: Lectures on phase transitions and the renormalization group, Addison-Wesley, 1992.

Goldstein, M. L., Morris, S. A., and Yen, G. G.: Problems with fitting to the power-law distribution, The European Physical Journal B-Condensed Matter and Complex Systems, 41, 255–258, 2004.

Golitsyn, G. S.: Place of the Gutenberg-Richter Law Among Other Statistical Laws of Nature, Vychislitel'naya Seysmologiya, 32, 119–137, 2001.

Golitsyn, G. S.: Energy cycle of geodynamics and the seismic process, Izvestiya, Physics of the Solid Earth, 43, 443–446, 2007.

Goodfellow, S. and Young, R.: A laboratory acoustic emission experiment under in situ conditions, Geophysical Research Letters, 41, 3422–3430, 2014.

Gutenberg, B. and Richter, C. F.: Earthquake magnitude, intensity, energy, and acceleration: (Second paper), Bulletin of the seismological society of America, 46, 105–145, 1956.

Harris, C. R., Millman, K. J., van der Walt, S. J., Gommers, R., Virtanen, P., Cournapeau, D., Wieser, E., Taylor, J., Berg, S., Smith, N. J., Kern, R., Picus, M., Hoyer, S., van Kerkwijk, M. H., Brett, M., Haldane, A., del Río, J. F., Wiebe, M., Peterson, P., Gérard-Marchant, P., Sheppard, K., Reddy, T., Weckesser, W., Abbasi, H., Gohlke, C., and Oliphant, T. E.: Array programming with NumPy, Nature, 585, 357–362, https://doi.org/10.1038/s41586-020-2649-2, 2020.

Holtkamp, S. G., Pritchard, M., and Lohman, R.: Earthquake swarms in south america, Geophysical Journal International, 187, 128–146, 2011.

Houdayer, J. and Hartmann, A. K.: Low-temperature behavior of two-dimensional Gaussian Ising spin glasses, Physical Review B, 70, 014 418, 2004.

Huilgol, R. R. and Phan-Thien, N.: Fluid mechanics of viscoelasticity: general principles, constitutive modelling, analytical and numerical techniques, Elsevier, 1997.

Ide, S., Beroza, G. C., Shelly, D. R., and Uchide, T.: A scaling law for slow earthquakes, Nature, 447, 76–79, 2007.

https://doi.org/10.5194/egusphere-2026-3399
Preprint. Discussion started: 19 June 2026

Ito, Y., Obara, K., Shiomi, K., Sekine, S., and Hirose, H.: Slow earthquakes coincident with episodic tremors and slow slip events, Science, 315, 503–506, 2007.

Janićević, S., Laurson, L., Måløy, K. J., Santucci, S., and Alava, M. J.: Interevent correlations from avalanches hiding below the detection threshold, Physical review letters, 117, 230 601, 2016.

Jones, L. M. and Molnar, P.: Some characteristics of foreshocks and their possible relationship to earthquake prediction and premonitory slip on faults, Journal of Geophysical Research: Solid Earth, 84, 3596–3608, 1979.

Kadanoff, L. P.: Scaling laws for Ising models near T_c, Physics Physique Fizika, 2, 263, 1966.

Kagan, Y. Y.: Seismicity: Turbulence of solids, Nonlinear Sci. Today, 2, 1–13, 1992.

Kagan, Y. Y.: Observational evidence for earthquakes as a nonlinear dynamic process, Physica D: Nonlinear Phenomena, 77, 160–192, 1994.

Kagan, Y. Y.: Seismic moment distribution revisited: I. Statistical results, Geophysical Journal International, 148, 520–541, https://doi.org/10.1046/j.1365-246x.2002.01594.x, 2002.

Kagan, Y. Y. and Knopoff, L.: Spatial distribution of earthquakes: the two-point correlation function, Geophysical Journal International, 62, 303–320, 1980.

Kanamori, H. and Anderson, D. L.: Theoretical basis of some empirical relations in seismology, Bulletin of the seismological society of America, 65, 1073–1095, 1975.

Kato, A., Obara, K., Igarashi, T., Tsuruoka, H., Nakagawa, S., and Hirata, N.: Propagation of slow slip leading up to the 2011 Mw 9.0 Tohoku-Oki earthquake, Science, 335, 705–708, 2012.

King, G. and Cocco, M.: Fault interaction by elastic stress changes: New clues from earthquake sequences, in: Advances in geophysics, vol. 44, pp. 1–VIII, Elsevier, 2001.

King, G. C., Stein, R. S., and Lin, J.: Static stress changes and the triggering of earthquakes, Bulletin of the Seismological Society of America, 84, 935–953, 1994.

Klein, E., Duputel, Z., Zigone, D., Vigny, C., Boy, J.-P., Doubre, C., and Meneses, G.: Deep transient slow slip detected by survey GPS in the region of Atacama, Chile, Geophysical research letters, 45, 12–263, 2018.

Kolmogórov, A.: Dissipation of energy in locally isotropic turbulence, in: Doklady Akademii Nauk, vol. 32, pp. 16–18, 1941a.

Kolmogórov, A.: The local structure of turbulence in incompressible viscous fluid for very large Reynolds numbers, in: Doklady Akademii Nauk, vol. 30, pp. 299–303, SSSR, 1941b.

Kossobokov, V. and Mazhkenov, S.: On similarity in the spatial distribution of seismicity, Computational seismology and geodynamics, 1, 6–15, 1994.

Kostrov, V.: Seismic moment and energy of earthquakes, and seismic flow of rock, Physics of the Solid Earth, 1, 13–21, 1974.

Lomnitz, C.: Major earthquakes and tsunamis in Chile during the period 1535 to 1955, Geologische Rundschau, 59, 938–960, 1970.

Lomnitz, C.: Major earthquakes of Chile: a historical survey, 1535-1960, Seismological Research Letters, 75, 368–378, 2004.

Madariaga, R.: On the relation between seismic moment and stress drop in the presence of stress and strength heterogeneity, Journal of Geophysical Research: Solid Earth, 84, 2243–2250, 1979.

Madariaga, R.: Earthquake source theory, Encyclopedia of Solid Earth Geophysics, pp. 1–5, 2020.

Main, I. G.: Statistical physics, seismogenesis, and seismic hazard, Reviews of Geophysics, 34, 433–462, 1996.

Main, I. G. and Burton, P. W.: Information theory and the earthquake frequency-magnitude distribution, Bulletin of the Seismological Society of America, 74, 1409–1426, 1984.

McComb, W. D.: Renormalization methods: a guide for beginners, OUP Oxford, 2003.

https://doi.org/10.5194/egusphere-2026-3399
Preprint. Discussion started: 19 June 2026

Mendecki, A. J.: Seismic monitoring in mines, Springer Science & Business Media, 1996.

Métois, M., Socquet, A., Vigny, C., Carrizo, D., Peyrat, S., Delorme, A., Maureira, E., Valderas-Bermejo, M.-C., and Ortega, I.: Revisiting the North Chile seismic gap segmentation using GPS-derived interseismic coupling, Geophysical Journal International, 194, 1283–1294, 2013.

Mignan, A. and Woessner, J.: Estimating the magnitude of completeness for earthquake catalogs, Community Online Resource for Statistical Seismicity Analysis, pp. 1–45, 2012.

Mueller, C. S.: Earthquake catalogs for the USGS national seismic hazard maps, Seismological Research Letters, 90, 251–261, 2019.

Neteler, M., Bowman, M., Landa, M., and Metz, M.: GRASS GIS: a multi-purpose Open Source GIS, Environmental Modelling & Software, 31, 124–130, https://doi.org/10.1016/j.envsoft.2011.11.014, 2012.

Nishikawa, T. and Ide, S.: Earthquake size distribution in subduction zones linked to slab buoyancy, Nature Geoscience, 7, 904–908, 2014.

Norabuena, E., Leffler-Griffin, L., Mao, A., Dixon, T., Stein, S., Sacks, I. S., Ocola, L., and Ellis, M.: Space Geodetic Observations of Nazca-South America Convergence Across the Central Andes, Science, 279, 358–362, https://doi.org/10.1126/science.279.5349.358, 1998.

Ogata, Y.: Statistical models for earthquake occurrences and residual analysis for point processes, Journal of the American Statistical association, 83, 9–27, 1988.

Okubo, P. G. and Aki, K.: Fractal geometry in the San Andreas fault system, Journal of Geophysical Research: Solid Earth (1978–2012), 92, 345–355, 1987.

Omori, F.: On the after-shocks of earthquakes, J. Coll. Sci., Imp. Univ., Japan, 7, 111–200, 1894.

Ott, E.: Chaos in dynamical systems, Cambridge university press, 2002.

Pastén, D. and Comte, D.: Multifractal analysis of three large earthquakes in Chile: Antofagasta 1995, Valparaiso 1985, and Maule 2010, Journal of seismology, 18, 707–713, 2014.

Poulos, A., Monsalve, M., Zamora, N., and de la Llera, J. C.: An updated recurrence model for Chilean subduction seismicity and statistical validation of its Poisson nature, Bulletin of the Seismological Society of America, 109, 66–74, 2019.

Ranero, C. R., von Huene, R., Weinrebe, W., and Reichert, C.: Tectonic processes along the Chile convergent margin, in: The Andes: Active Subduction Orogeny, pp. 91–121, Springer, 2006.

Rapp, B. E.: Microfluidics: modeling, mechanics and mathematics, William Andrew, 2016.

Ruiz, S. and Madariaga, R.: Historical and recent large megathrust earthquakes in Chile, Tectonophysics, 733, 37–56, 2018.

Ruiz, S., Metois, M., Fuenzalida, A., Ruiz, J., Leyton, F., Grandin, R., Vigny, C., Madariaga, R., and Campos, J.: Intense foreshocks and a slow slip event preceded the 2014 Iquique Mw 8.1 earthquake, Science, p. 1256074, 2014.

Scholz, C. H. and Aviles, C. A.: The Fractal Geometry of Faults and Faulting, pp. 147–155, American Geophysical Union (AGU), ISBN 9781118664865, https://doi.org/10.1029/GM037p0147, 1986.

Sedov, L. I.: Similarity and dimensional methods in mechanics, CRC press, 1993.

Serra, I. and Corral, Á.: Deviation from power law of the global seismic moment distribution, Scientific reports, 7, 1–8, 2017.

Siegel, C. E., Toledo, P., Madariaga, R., and Campos, J.: Scaling of waiting time distribution in northern Chile, ESS Open Archive, 10.1002/essoar.10508115.3, 2022.

Sobiesiak, M. M.: Fault plane structure of the Antofagasta, Chile earthquake of 1995, Geophysical research letters, 27, 577–580, 2000.

Socquet, A., Valdes, J. P., Jara, J., Cotton, F., Walpersdorf, A., Cotte, N., Specht, S., Ortega-Culaciati, F., Carrizo, D., and Norabuena, E.: An 8 month slow slip event triggers progressive nucleation of the 2014 Chile megathrust, Geophysical Research Letters, 44, 4046–4053, 2017.

https://doi.org/10.5194/egusphere-2026-3399
Preprint. Discussion started: 19 June 2026

Tian, D., Uieda, L., Leong, W. J., Schlitzer, W., Fröhlich, Y., Grund, M., Jones, M., Toney, L., Yao, J., Magen, Y., Tong, J.-H., Materna, K., Belem, A., Newton, T., Anant, A., Ziebarth, M., Quinn, J., and Wessel, P.: PyGMT: A Python interface for the Generic Mapping Tools, https://doi.org/10.5281/zenodo.8303186, 2023.

Tsuboi, C.: Isostasy and maximum earthquake energy, Proceedings of the Imperial Academy, 16, 449–454, 1940.

Tsuboi, C.: Earthquake energy, earthquake volume, aftershock area, and strength of the Earth's crust, Journal of Physics of the Earth, 4, 63–66, 1956.

Uchida, N. and Matsuzawa, T.: Pre-and postseismic slow slip surrounding the 2011 Tohoku-oki earthquake rupture, Earth and Planetary Science Letters, 374, 81–91, 2013.

Udías, A., Madariaga, R., Buforn, E., Muñoz, D., and Ros, M.: The large Chilean historical earthquakes of 1647, 1657, 1730, and 1751 from contemporary documents, Bulletin of the Seismological Society of America, 102, 1639–1653, 2012.

Utsu, T., Ogata, Y., and Matsu'ura, R. S.: The centenary of the Omori formula for a decay law of aftershock activity, Journal of Physics of the Earth, 43, 1–33, 1995.

Vargas, G., Klinger, Y., Rockwell, T., Forman, S., Rebolledo, S., Baize, S., Lacassin, R., and Armijo, R.: Probing large intraplate earthquakes at the west flank of the Andes, Geology, 42, 1083–1086, 2014.

Virkar, Y. and Clauset, A.: Power-law distributions in binned empirical data, The Annals of Applied Statistics, 8, 90–119, http://www.jstor.org/stable/24521727, 2014.

Wessel, P., Luis, J., Uieda, L., Scharroo, R., Wobbe, F., Smith, W., and Tian, D.: The Generic Mapping Tools version 6, Geochemistry, Geophysics, Geosystems, 20, 5556–5564, 2019.

Widom, B.: Scaling laws, Scholarpedia, 4, 9054, https://doi.org/10.4249/scholarpedia.9054, 2009.

Wilson, K. G.: The renormalization group: Critical phenomena and the Kondo problem, Reviews of modern physics, 47, 773, 1975.

Wilson, K. G.: Problems in physics with many scales of length, Scientific American, 241, 158–179, 1979.

Yoshimitsu, N., Kawakata, H., and Takahashi, N.: Magnitude- 7 level earthquakes: A new lower limit of self-similarity in seismic scaling relationships, Geophysical Research Letters, 41, 4495–4502, 2014.

Zel'dovich, J. B.: The motion of a gas under the action of a short-term pressure shock, Soviet Physics Acoustics, 2, 25–35, 1956.

Zorich, V.: Mathematical analysis of problems in the natural sciences, Springer Science & Business Media, 2010.